UNCLASSIFIED

SECURITY CLASSIFICATION OF THIS PAGE (When Data Entered)

REPORT DOCUMENTATION PAGE

READ INSTRUCTIONS BEFORE COMPLETING FORM

1. REPORT NUMBER: AFIT/CI/NR 88-86
2. GOVT ACCESSION NO.:
3. RECIPIENT'S CATALOG NUMBER:
4. TITLE (and Subtitle): ATMOSPHERIC CORRECTIONS FOR IN-FLIGHT SATELLITE RADIOMETRIC CALIBRATION
5. TYPE OF REPORT & PERIOD COVERED: MS THESIS
6. PERFORMING ORG. REPORT NUMBER:
7. AUTHOR(s): RICHARD JOSEPH BARTELL
8. CONTRACT OR GRANT NUMBER(s):
9. PERFORMING ORGANIZATION NAME AND ADDRESS: AFIT STUDENT AT: UNIVERSITY OF ARIZONA
10. PROGRAM ELEMENT, PROJECT, TASK AREA & WORK UNIT NUMBERS:
11. CONTROLLING OFFICE NAME AND ADDRESS:
12. REPORT DATE: 1988
13. NUMBER OF PAGES: 100
14. MONITORING AGENCY NAME & ADDRESS (if different from Controlling Office): AFIT/NR, Wright-Patterson AFB OH 45433-6583
15. SECURITY CLASS. (of this report): UNCLASSIFIED
15a. DECLASSIFICATION/DOWNGRADING SCHEDULE:
16. DISTRIBUTION STATEMENT (of this Report): DISTRIBUTED UNLIMITED: APPROVED FOR PUBLIC RELEASE

17. DISTRIBUTION STATEMENT (of the abstract entered in Block 20, if different from Report): SAME AS REPORT
18. SUPPLEMENTARY NOTES: Approved for Public Release: IAW AFR 190-1
LYNN E. WOLAVER 19 July 88
Dean for Research and Professional Development
Air Force Institute of Technology
Wright-Patterson AFB OH 45433-6583
19. KEY WORDS (Continue on reverse side if necessary and identify by block number):
20. ABSTRACT (Continue on reverse side if necessary and identify by block number): ATTACHED

88

DD FORM 1 JAN 73 1473 EDITION OF 1 NOV 65 IS OBSOLETE

UNCLASSIFIED

SECURITY CLASSIFICATION OF THIS PAGE (When Data Entered)

ATMOSPHERIC CORRECTIONS FOR IN-FLIGHT SATELLITE RADIOMETRIC CALIBRATION

Richard Joseph Bartell
Captain, USAF
1987
100 pp.
Master of Science
The University of Arizona

Accurate determination of atmospheric effects is crucial to earth-based in-flight radiometric calibration of existing satellite systems. Such calibration work relies on computer codes which compute atmospheric transmittance due to both scattering and absorption processes. Two programs evaluated in this paper are 5S, the Simulation of the Satellite Signal in the Solar Spectrum, and LOWTRAN 6.

Two solar radiometers of differing designs were used for atmospheric data collection. The collected data were used to compute total optical depths. Results obtained from the two instruments in the visible are compared. Modifications made to the autotracking instrument are discussed.

The accuracy of existing methods for determining the amounts of key constituents actually present in the atmosphere at satellite overpass time is examined. The computation of integrated water vapor content based on solar radiometer data is discussed.

Calculations to account for the effects of gaseous absorption in the near infrared spectral bands of a solar radiometer are outlined. Such corrections will facilitate calibration of these spectral bands.

In conclusion, the effects on radiance at the satellite level of the uncertainties in the current determination of crucial atmospheric parameters such as the extent of gaseous absorption and the aerosol characterization are examined. (Theses; jhal)

ATMOSPHERIC CORRECTIONS FOR IN-FLIGHT SATELLITE RADIOMETRIC CALIBRATION

by

Richard Joseph Bartell

A Thesis Submitted to the Faculty of the

COMMITTEE ON OPTICAL SCIENCES (GRADUATE)

In Partial Fulfillment of the Requirements
For the Degree of

MASTER OF SCIENCE

In the Graduate College

THE UNIVERSITY OF ARIZONA

1 9 8 7

STATEMENT BY AUTHOR

This thesis has been submitted in partial fulfillment of requirements for an advanced degree at the The University of Arizona and is deposited in the University Library to be made available to borrowers under rules of the Library.

Brief quotations from this thesis are allowable without special permission, provided that accurate acknowledgment of source is made. Requests for permission for extended quotation from or reproduction of this manuscript in whole or in part may be granted by the head of the major department or the Dean of the Graduate College when in his or her judgment the proposed use of the material is in the interests of scholarship. In all other instances, however, permission must be obtained from the author.

SIGNED: Richard J Bartell

APPROVAL BY THESIS DIRECTOR

This thesis has been approved on the date shown below:

P. N. Slater
Professor of Optical Sciences

10 December 1987
Date

ACKNOWLEDGMENTS

The author would like to take this opportunity to pay tribute to the many people who made this work possible. I would like to thank Dr. Philip N. Slater for allowing me to join his group and for bearing with me when things were not going smoothly. I would also like to thank my co-workers, Stuart Biggar and Benfan Yuan, whose help and comments, especially those concerning the equipment and software, have been truly invaluable. I would like to pay a very special thanks to Dr. Richard P. Santer of Universite' des Sciences et Techniques de Lille, France, who so superbly directed this research.

Additionally, I would like to thank Dr. Ray Jackson and Ms. M. Susan Moran of the Water Conservation Laboratory for their assistance and helpful discussions and with whom it was a pleasure to conduct field measurements over the course of this research.

I would like to especially thank my parents and grandparents for all the help and encouragement over the years. Without them, none of this would have been possible.

Most importantly, I would like to thank my wife Melissa for her expert proofreading, general insightful comments and for putting up with me during the long months this manuscript was in preparation.

TABLE OF CONTENTS

TABLE OF CONTENTS--Continued

TABLE OF CONTENTS--Continued

LIST OF ILLUSTRATIONS

LIST OF ILLUSTRATIONS--Continued

LIST OF TABLES

LIST OF TABLES--Continued

Page

Table

ABSTRACT

Accurate determination of atmospheric effects is crucial to earth-based in-flight radiometric calibration of existing satellite systems. Such calibration work relies on computer codes which compute atmospheric transmittance due to both scattering and absorption processes.

Two solar radiometers were used for atmospheric data collection. Results obtained from the two instruments in the visible are compared. Modifications to the autotracking instrument are discussed.

The accuracy of existing methods for determining the amounts of key atmospheric constituents actually present at a given time is examined. Computation of integrated water vapor content based on solar radiometer data is discussed.

Calculations to account for the effects of gaseous absorption in the near infrared spectral bands of a solar radiometer are outlined. Such corrections will facilitate calibration of these spectral bands.

In conclusion, the effects of the uncertainties in the current determination of crucial atmospheric parameters on radiance at the satellite level are examined.

CHAPTER 1

INTRODUCTION

The purpose of this study was to improve determination of atmospheric effects on the radiative transfer process as it pertains to the problem of in-flight satellite radiometric calibration. This problem includes both the visible and near-infrared (IR) portions of the spectrum, those wavelengths utilized by Landsat's Thematic Mapper (TM), the French "Systeme Probatoire d'Observation de la Terre" (SPOT) satellite, and the Advanced Very High Resolution Radiometer (AVHRR) carried by NOAA 9 and 10. The work outlined in this paper centers on attempts to improve both an existing instrument and analysis of its data in order to more accurately determine the amount of atmospheric scattering and absorption modifying the incident exoatmospheric solar radiation.

Initially, it is useful to define the basic composition of the atmosphere and the effects those constituents have on incident solar radiation as it passes through the atmosphere.

General Theory

Atmospheric Constituents

The earth's atmosphere is a very complex mixture of gases and suspended particles, or aerosols. The gaseous components of the atmosphere are well-defined and for these purposes can be considered to include H_2O, O_3, CO_2, N_2O, CO, O_2, CH_4, and N_2. The trace components are ignored since they have negligible effect on the process of radiative transfer. According to McClatchey et al. (1972), CO_2, N_2O, CO, O_2, CH_4, and N_2 are considered to be uniformly mixed by

volume. It has been determined that the amount of CO_2 in the atmosphere has actually been slowly increasing since the onset of the Industrial Revolution (Liou 1980, p.117). For most purposes, though, the amount of CO_2 in the atmosphere can be considered constant.

The aerosols are composed of particles ranging in size from 10^{-9} meters to 10^{-4} meters in diameter (Iqbal 1983, p.96). The particles are dispersed in the atmosphere from a number of different sources. These include industrial smoke, oceanic salts, volcanic dust, desert sand, smoke from forest and other large fires, etc (Iqbal 1983, p.95). Due to the nature of the aerosols, their number density and size distribution in the atmosphere change constantly.

Atmospheric Attenuation

The two atmospheric attenuation mechanisms are scattering and absorption of the incident radiation. The gaseous, or molecular, and aerosol constituents each have an associated scattering and absorption coefficient.

Scattering by molecules is referred to as Rayleigh scattering, after Lord Rayleigh who first derived a mathematical expression to describe it. The Rayleigh determination assumes the molecules are pure scatterers. This assumption is valid for both oxygen and nitrogen, which together account for 99 percent of all molecular scattering by virtue of their predominance in the composition of the atmosphere (McCartney 1976). Rayleigh scattering is proportional to λ^{-4} and therefore dominant at the shorter wavelengths. Rayleigh scattering explains the blue hue of the daytime sky. This is in contrast to scattering of radiation by the suspended aerosols, where the wavelength dependence is approximately λ^{-1}. This scattering by larger particles, with radii up to 100 μm, produces a strong forward component and is referred to as Mie scattering (van de Hulst 1957).

The amount of atmospheric attenuation experienced by the incident solar radiation at any given wavelength is expressed by a dimensionless quantity known as optical depth. In the expression of Beer's Law, which is monochromatic in nature and describes atmospheric transmittance in the absence of absorption,

$$E_\delta = E_0 \, e^{-m\delta} \qquad (1.1)$$

E_δ is the observed irradiance,
E_0 is the exoatmospheric solar spectral irradiance,
δ is the optical depth,
and m is the airmass.

In equation (1.1) airmass is defined as the secant of the solar zenith angle. For complete accuracy at large solar zenith angles, the sphericity of the atmosphere and related refraction effects must be taken into account when calculating airmass (Kneizys et al. 1983). Airmass has a minimum value of one when the sun is vertically overhead and a maximum value for data collection purposes dictated by when the sun rises above the local horizon.

The optical depth in equation (1.1) is the total optical depth, which at any wavelength is simply the sum of the component optical depths due to Rayleigh scattering, attenuation due to aerosols and, where applicable, attenuation due to ozone absorption. Typical values for total optical depth range from approximately 0.6 at 0.4 μm to 0.04 at 1.04 μm for the non-turbid air in the Arizona region.

Atmospheric Variability

Perhaps the greatest problem in dealing with the question of atmospheric attenuation is the constantly changing nature of the atmosphere itself. Even in a short period of time the atmospheric make-up can change substantially.

The molecular scattering component depends directly on atmospheric surface pressure and so can change suddenly, although not greatly, with the passage

of a weather front. The amount of the uniformly mixed gasses present, and therefore the amount of associated absorption, also depends directly on atmospheric pressure.

Ozone content varies rather slowly and predictably over the course of the year and depends heavily on the latitude of the observer (Junge 1963).

The atmospheric constituents which can change concentrations or distribution most rapidly are the aerosols and water vapor. The water vapor content in a vertical column of air can be approximately determined using data collected by a radiosonde. However, a value so determined is only valid for the time close to that of the radiosonde ascent. There are also relatively few ground stations which launch radiosondes at the present time. An accurate alternate method of determining atmospheric water vapor content at a specific time is highly desirable. The direct measurement of aerosol content using impactors is seldom practical, but has been accomplished on occasion (Lindberg and Gillespie 1978). The atmospheric aerosol number density and size distribution can be prone to rapid fluctuations and unfortunately must almost always be inferred from measurements of the optical depth.

The proper determination of atmospheric optical depths at selected wavelengths is therefore crucial for calculating the contribution of the various atmospheric constituents in the attenuation process.

Related Background Work

During this work, data collection for the determination of optical depth involved two instruments. One was a relatively new solar spectroradiometer capable of computer controlled operation for extended periods of time. This instrument, designed and built by Dr. Kenneth R. Castle while at the University of Arizona, will be referred to as the Autotracker. The other instrument used was a

manually operated solar radiometer designed by Dr. John A. Reagan of the University of Arizona, referred to as the Reagan instrument. Because of its long-term reliability, the Reagan instrument results are used to verify the proper operation of the Autotracker.

From data collected with each instrument, the optical depths for a given day were determined using the Langley-Bouguer technique in which the natural logarithm of the measured irradiance is plotted against the corresponding airmass. This technique yields the total optical depth or extinction for each wavelength for which data were collected.

In order to properly account for absorption and scattering effects in the spectral bands of the satellites, which do not correspond directly to those of the ground-based instruments, the actual amounts of the various absorbers present in the atmosphere must be determined.

It is possible to compute values for the amounts of absorbers present during a given observation period using measurements taken with the ground-based instruments. The following section provides an overview of the Autotracker's design and outlines how these ground based measurements are made.

The Autotracker

The Autotracker is a spectropolarimeter mounted on an altitude/azimuth platform. It has the capability of taking measurements in twelve spectral bands, ranging in central wavelength from 0.42 μm to 2.25 μm. The individual bands are isolated using normal incidence interference filters, with the bandwidths varying from 10 nanometers (nm) in the visible to over 200 nm in the near IR. Table 1.1 lists the central wavelengths and bandwidths for each of the Autotracker's twelve bands. These values are computed from measurements of filter response made in

the fall of 1986. The bandwidths and central wavelengths were computed using the Palmer moments method (Palmer and Tomasko 1980).

Table 1.1 The Autotracker's Spectral Bands

Band	Central λ (μm)	Bandwidth (μm)
Silicon Detector:		
1	0.4214	0.0109
2	0.4407	0.0119
3	0.5255	0.0104
4	0.6054	0.0108
5	0.6615	0.0106
6	0.7803	0.0121
7	0.8619	0.0152
8	0.9496	0.0247
9	1.0427	0.0230
Lead Sulfide Detector:		
7	0.8619	0.0152
8	0.9496	0.0247
9	1.0427	0.0230
10	1.6461	0.2174
11	2.2058	0.2438
12	2.2453	0.0514

Through use of four neutral density filters, a dynamic range of 10^4 is achieved. The instrument's angular field of view (FOV) is defined by a field stop at the focus of the objective lens. With this design, the FOV is selectable, with 1°, 2°, and 5° FOV's available. A 2° FOV has been the standard for solar tracking operations due to concern that the solar tracking process was not sufficiently accurate to support use of the 1° FOV.

The spectral range of 0.42 μm to 2.25 μm is covered using two detectors. The first is a silicon photodiode detector used in nine bands in the visible and near IR from 0.42 μm to 1.04 μm. The second detector is a lead sulfide detector, used in six near-IR bands from 0.86 μm to 2.25 μm. The two detectors have three common spectral bands at 0.86 μm, 0.95 μm, and 1.04 μm. The

detectors are mounted in a common sliding mount and are heated to approximately 48° C. The common mount arrangement allows the detectors to use the same optics. Figure 1.1 is a schematic of the Autotracker's radiometer.

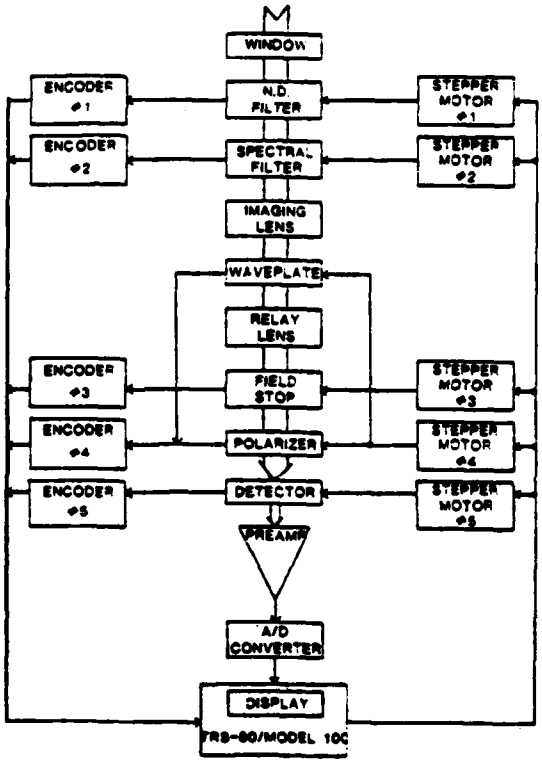

Figure 1.1 Schematic of the Autotracker's Radiometer, Castle (1985)

Solar tracking and data collection are accomplished by a lap-top computer. The tracking program currently used is based on a 22-term low precision Chebyshev polynomial series. The Chebyshev coefficients are extracted from the Almanac for Computers (1987). The radiometer's positioning is accomplished by two mutually perpendicular stepper motor-driven precision turntables and is updated every 12 seconds when the instrument is in use (Slater et al. 1987). A data collection cycle begins every three minutes and the data are written to a double-sided 3.5 inch disk. This arrangement enables the Autotracker

to operate uninterrupted for over nine hours. Previously data were stored on the lap-top computer itself, creating problems due to memory limitations.

The Reagan solar radiometer is a completely manual instrument using a single spectral filter wheel and a single silicon detector. It utilizes ten spectral bands between 0.37 μm and 1.03 μm.

The Autotracker and Reagan instrument data are read and converted into files of detector output voltage and airmass values. These files are then used to produce Langley-Bouguer plots for each spectral band.

The Langley-Bouguer Plot Technique

The Langley-Bouguer plot technique, as mentioned earlier, is a graphical method of determining total optical depths. By taking the natural logarithm of both sides of equation (1.1), the expression for Beer's Law, we have,

$$\ln E_\delta = \ln E_o - m\delta \quad . \qquad (1.2)$$

From equation (1.2) it is obvious that the slope of a Langley-Bouguer plot is the optical depth and the intercept of a Langley-Bouguer plot created using data obtained from an absolutely calibrated instrument provides the exoatmospheric solar irradiance. An absolutely calibrated instrument is one for which the relationship between E_δ and output voltage is known. Such a calibration was accomplished for the Autotracker's original nine spectral bands in 1985 (Castle 1985). However, the instrument has undergone several major modifications since then and this calibration can no longer be considered accurate. This has no effect on the calculation of optical depths; it only affects the intercept values. The two primary conditions necessary for a valid Langley-Bouguer plot are a large range of airmass values, typically from 1.5 to at least 5, and a stable, cloudless atmosphere throughout the measurement period. Figure 1.2 is an example of a typical Langley-Bouguer plot. The slight irregularity in the plotted data is commonly observed.

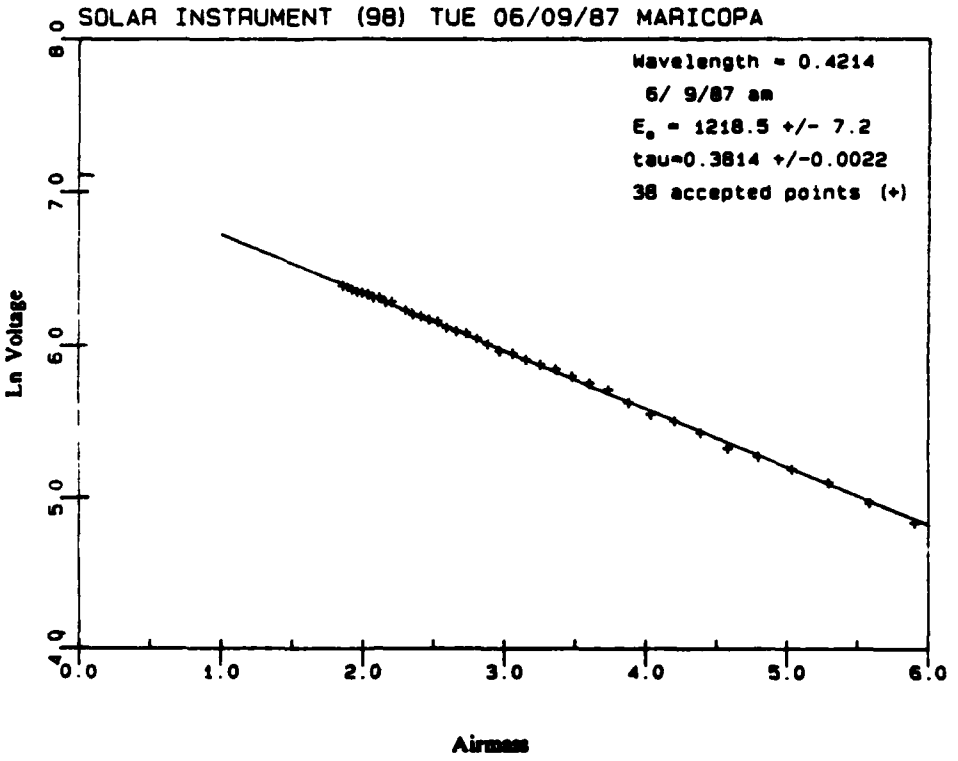

Figure 1.2 Typical Langley-Bouguer Plot

In the section on atmospheric corrections it will be shown that Beer's Law is actually only valid for a non-absorbing, non-scattering atmosphere. Therefore, before applying the Langley-Bouguer plot technique it is necessary to know whether the condition of no absorption is met in the spectral band of interest. Scattering, at least that due to molecules, will occur under all conditions.

Determination of Atmospheric Gaseous/Aerosol Content

As mentioned in the section on General Theory, atmospheric gaseous molecules and aerosols exhibit both scattering and absorbing behavior. A mathematical definition of optical depth at a given elevation, $\delta(z)$, is,

$$\delta(z) = \int_z^\infty k_T \rho dz \qquad (1.3)$$

where z is elevation of the observation point,
k_T is the total attenuation coefficient,
and ρ is the density of the medium.

The total attenuation coefficient at any wavelength can be considered to be composed of molecular and aerosol components (McClatchey et al. 1972).

Rayleigh, or molecular, scattering is present at all wavelengths. Rayleigh optical depth, δ_{Ray}, can be approximately determined using the following expression given surface atmospheric pressure (Elterman 1968 and Kastner 1985),

$$\delta_{Ray} = \frac{8\pi^3(n^2-1)^2}{3\lambda^4(N_S)^2} \frac{6+3\gamma}{6-7\gamma} N_C \, 10^{16} \frac{P}{P_0} \qquad (1.4)$$

where n is the refractive index,
λ is the wavelength in μm,
N_S is 2.547 x 10^{19} cm^{-3}, the sea level molecular number density,
N_C is 2.154 x 10^{25} cm^{-2}, the columnar number density,
γ equals 0.035, an anisotropic correction factor,
P_0 is standard pressure (1013.25 mb),
and P is actual atmospheric pressure.

In order to accurately determine the contribution of molecular absorption to the total attenuation, the actual quantities of the absorbers present in the atmosphere must be calculated. However, it is important to know that attenuation due to molecular absorption can be avoided to a large degree by careful selection of spectral bands used for measurements, using the atmospheric windows. Unfortunately, even the atmospheric windows are affected to some extent by gaseous absorption. The Autotracker's first nine spectral bands were selected so that some were in regions of no absorption while others were in ozone and water vapor

absorption bands. The Autotracker bands selected in the regions of absorption can allow an accurate determination of actual ozone and water vapor content. Knowing these concentrations, necessary corrections can be applied to the various satellite bands. Specific methods to determine ozone and water vapor content from Autotracker data will be outlined in Chapter 3.

Table 1.2 lists some representative values for gaseous transmittance in each of the Autotracker's spectral bands for an airmass of approximately 3.5. The transmission values were generated using a standard atmospheric transmission computer code and represent integration over the bandpass of each filter. The computer code used in this case was 5S, which will be discussed in some detail in later chapters. The Mid-Latitude Summer atmospheric model, which assumes a total integrated water vapor content of 2.93 g/cm^2 and a total ozone content of 0.319 atm-cm was used for the calculation. The varying effect of gaseous absorption is evident.

Table 1.2 Representative Transmittance Values for the Autotracker's Spectral Bands for a Complete Path Through the Atmosphere

Band:	1	2	3	4	5	6
Global	1.0	0.998	0.944	0.861	0.915	0.999
H_2O	1.0	1.0	1.0	0.985	0.971	0.999
O_3	1.0	0.998	0.944	0.874	0.942	1.0
CO_2	1.0	1.0	1.0	1.0	1.0	1.0
Band:	**7**	**8**	**9**	**10**	**11**	**12**
Global	0.991	0.189	0.999	0.924	0.894	0.973
H_2O	0.991	0.189	0.999	0.937	0.907	0.973
O_3	1.0	1.0	1.0	1.0	1.0	1.0
CO_2	1.0	1.0	1.0	0.986	0.986	1.0

The effect at the satellite level due to attenuation from scattering by aerosols, referred to as Mie scattering, and absorption by these aerosols can be calculated for any wavelength in the visible spectrum by a radiative transfer code. Radiative transfer codes will be discussed specifically in the next section, however Autotracker or Reagan instrument optical depths are a necessary input. In using these optical depths as input, it is assumed at the present that the aerosols closely follow a Junge radial size distribution described by,

$$n(r) = \frac{dN}{N\,dr} = Cr^{-(\nu+1)} \qquad (1.5)$$

where N is the number of particles per unit volume, C is a constant and ν is a parameter describing the distribution (Junge 1963). For each particular case, the Junge parameter ν must be determined. One method of determining ν is through calculation of the Ångström wavelength exponent. The Ångström wavelength exponent is calculated from measurements made primarily in the visible as follows: for wavelengths where there are no absorption effects, specifically in this case Autotracker Bands 2 and 7, Mie optical depth, δ_{Mie}, is found by subtracting the calculated Rayleigh optical depth from the total optical depth found using the Langley-Bouguer plot. The Mie optical depth represents the total attenuation due to aerosols. Then, on a plot of log δ_{Mie} versus log λ, a line is drawn through these two points. The slope of this line is the Ångström wavelength exponent (α). This technique is based on the following three equations. The first is the expression relating aerosol optical depth and wavelength developed by Ångström,

$$\delta_{Mie}(\lambda) = a\lambda^{-\alpha} \qquad (1.6)$$

where a is a turbidity coefficient. δ_{Mie} at any wavelength can also be defined in terms of the aerosol size distribution and particle extinction by,

$$\delta_{Mie}(\lambda) = \int_0^\infty \pi r^2 Q_{ext}((r/\lambda),m)n(r)dr \qquad (1.7)$$

where r is the particle radius, Q_{ext} is the extinction efficiency and m is the refractive index. By defining $\alpha = 2\pi r/\lambda$ and substituting the expression for n(r) found in equation (1.5) into equation (1.7), the following result can be obtained,

$$\delta_{Mie}(\lambda) = c(\lambda/2\pi)^{-\nu+2}\int_0^\infty Q_{ext}(\alpha,m)\ \alpha^{-\nu+1}\ d\alpha \quad . \qquad (1.8)$$

Thus the Junge parameter ν, known as the Junge size distribution, equals the Ångström wavelength exponent plus two (van de Hulst 1957). The Junge parameter ν is a necessary input to the radiative transfer codes for the computation of the scattering phase function. Furthermore, once α is known, a theoretical value for δ_{Mie} at any wavelength can be easily computed based on equation (1.6).

Atmospheric Corrections

The purpose of determining accurate values for the concentrations of molecular absorbers and the aerosol size distribution is to allow calculation of the effect of the earth-atmosphere system on incident exoatmospheric solar radiation. Specifically, the purpose in this application was to allow calculation of the radiance at the entrance aperture of a satellite. The calculations necessary to correct for the effects of gaseous absorption and scattering into and out of the beam are known as atmospheric corrections (Slater 1980).

Scattering Process. The most difficult effects to calculate are those of scattering and absorption by aerosols. It is extremely important that these quantities be accurately determined since aerosols typically account for up to 70 percent of the optical depth in the first three kilometers above sea level (Elterman 1970). As mentioned in the previous section, these effects can only be accurately calculated by one of a class of computer programs which solve the radiative transfer equation numerically, known as radiative transfer codes. This type of solution has been available for some time.

A computer code representative of this type is one developed by Herman and Browning (1965). In this code, the equation of radiative transfer,

$$\frac{dL(\theta,\phi)}{-k_T\ \rho\ ds} = L(\theta,\phi) - J(\theta,\phi) \qquad (1.9)$$

where $L(\theta,\phi)$ is the source radiance,
$J(\theta,\phi)$ is the source function,
k_T is the total attenuation coefficient,
ρ is the density of the medium,
and ds is the distance traveled through the medium,

is solved using the Gauss-Seidel iterative technique. This form of the radiative transfer equation was taken from the discussion in Chandrasekhar (1960). It is important to note here that Beer's Law is a special case of the downward solution of the radiative transfer equation, one for which the source function is neglected. The source function accounts for the effects of scattering into and out of the direct solar beam. Therefore Beer's Law, as applied in the Langley-Bouguer technique, is actually only valid for small values of optical depths when there is little probability of multiple scattering taking place. In the Herman and Browning computer code the atmosphere is divided into layers thin enough that only single scattering can be assumed to occur in each layer, thus eliminating the complexities of multiple scattering.

The code runs in two parts, calculation of the scattering phase function followed by solution of the radiative transfer equation. Typical inputs necessary for such a code to compute the scattering phase function include the Junge size distribution, the largest and smallest aerosol particle size, the incremental radial size step, the real and imaginary parts of the aerosol refractive index and the wavelength of interest. An aerosol refractive index of 1.54-0.01i has been assumed in the satellite calibration work for which the code is used, based on the work of

Jennings et al. (1978). The imaginary part of the refractive index determines the amount of absorption due to aerosols. Using the above inputs, the scattering phase function is computed. To solve the radiative transfer equation the code requires the solar zenith angle, the surface reflectance value, the surface elevation and the three components of the optical depth for the wavelength in question. These three components of optical depth are due to molecular scattering, molecular absorption, and attenuation due to aerosols. The final result of the program is the fractional radiance reaching the entrance pupil of the satellite relative to unity incident exoatmospheric solar irradiance.

Since a primary input to a radiative transfer code is the optical depth due to gaseous absorption, it is important that the amount of gaseous absorption taking place in the spectral bands of the satellites be accurately determined.

Gaseous Absorption. If the actual concentration of gaseous absorbers present in the atmosphere can be accurately determined, there are several programs available which can be used to calculate gaseous absorption occurring at any desired wavelength.

The two programs used in this work were LOWTRAN 6, developed by Kneizys et al. (1983) of the U.S. Air Force Geophysics Laboratory and 5S, the Simulation of the Satellite Signal in the Solar Spectrum developed by Tanre' et al. (1986) of the Universite' des Sciences et Techniques de Lille, France. LOWTRAN has a resolution of 20 wavenumbers, which equals approximately 2 nm at a wavelength of 1 μm, as compared to a constant resolution of 5 nm for 5S.

Inputs for these programs include the solar zenith angle, the viewing angle, the bandwidth of spectral bands being considered, and the surface reflectance. The surface reflectance is required to compute the results of both an upward and downward pass. Also required as input is an atmospheric model. A

standard atmospheric model can be chosen or a user-defined one can be developed. It is the user-defined model option which allows input of actual atmospheric absorber concentrations, particularly ozone and water vapor.

The importance of accurate determination of inputs for both radiative transfer and atmospheric transmittance codes is obvious. Chapter 2 deals with efforts made to improve the calculation of optical depths in the visible portion of the spectrum using the Autotracker for data collection. The accuracy of these total optical depths in turn directly influences the calculation of the amounts of ozone and water vapor actually present.

CHAPTER 2

DETERMINATION OF TOTAL OPTICAL DEPTH

One of the overall goals of this work was to improve the reliability of the Autotracker and to refine reduction of its data so that optical depths determined using this instrument could be used in the absolute in-flight radiometric calibration of satellites. Since its inception the Autotracker has experienced problems from a variety of sources which have detracted from its overall data collection performance. A number of these problems have been identified and corrected. What follows first is an explanation of these individual problems and the steps taken to correct them. Secondly, the impact of errors or malfunctions during data collection on the calculation of optical depths using the Langley-Bouguer technique are explored. Lastly, attempted corrections of computed optical depths for temperature fluctuations of the detector and for the contribution of diffuse radiation scattered into the instrument's field of view are described.

Autotracker Data Acquisition Improvements

Optical depth determination with the Autotracker in the past has only been moderately successful. The problems experienced, for the most part, arose from mechanical failures or inconsistencies in its data collection operation. Modifications were made to the Autotracker's computer procedures to eliminate former limitations. Steps were also taken to eliminate possible sources of errors in the time reference and geographic position information necessary for data collection. Most importantly, corrections were made to several of the instrument's calibration

constants. The fact such corrections were necessary indicates possible changes with time in the instrument's optical system, particularly the filters used.

Time and Position References

In the effort to improve optical depth determination with the Autotracker, the first steps taken were to ensure that proper values were used for the time and geographic position references during data collection as errors in either of these could affect the results of the final data reduction.

For the time reference, Coordinated Universal Time as provided by WWV in Colorado was chosen, due to its well-established accuracy and the ease of acquisition, even at remote sites. The time the Autotracker takes data in each spectral band, as determined from the lap-top computer's internal clock, is written to the data file. These recorded times are used to calculate the appropriate value for airmass for that measurement by referencing solar ephemeris data. It is evident from the work done by Thomason et al. (1982), that in order to achieve one percent accuracy in zero airmass Langley-Bouguer plot intercepts for measurements taken in the southwestern United States, the actual time must be known to within a few seconds for airmass values above five. The tolerance increases significantly as the value for airmass drops. It is important that these intercepts be accurately determined for the purpose of calibrating the radiometer.

Also, the geographic coordinates for each of the satellite calibration data collection sites, as well as those of the Autotracker test location at the University of Arizona, were checked for accuracy. This was accomplished by locating the various sites on USGS topographic charts and determining their Universal Transverse Mercator (UTM) coordinates. The scale of these charts is typically 1:24,000, sufficient to see individual buildings. These UTM coordinates were then

converted to geographic coordinates based on the North American Datum of 1927 (NAD-27), which is the current horizontal reference for charts of the western United States. Coordinates determined in this manner are considered accurate to ±60 feet.

The geographic coordinates of a data collection site are entered into the solar tracking program with a precision of approximately ±300 feet. The error in the University site, for example, was found to be in excess of 1600 feet. However, results of a sensitivity analysis for a 2° FOV indicate longitude errors of up to 3 miles would not affect solar tracking during the time interval required to collect data for a valid Langley-Bouguer plot. Tracking accuracy is significantly less sensitive to latitude errors. Therefore, site coordinates do not appear to represent a significant source of error.

Some minor modifications were made to the Autotracker's computer equipment and software in an effort to eliminate possible causes of lost data and solar tracking errors.

Computer-Related Modifications

Originally Autotracker data were stored in the lap-top computer's Random Access Memory (RAM) during data collection. Due to memory limitations, the amount of data the lap-top computer could store corresponded to approximately two hours of data collection. At this two hour point, the original lap-top computer had to be replaced so that previously collected data would not be overwritten. This required that the solar tracking program be restarted using the replacement computer. When data collected using two or more computers were combined on a single Langley-Bouguer plot, the result was often a slight mismatch between the slopes and intercepts of the line segments corresponding to data collected with the

different computers. Figure 2.1 illustrates this effect, with the mismatch occurring around an airmass value of 1.7.

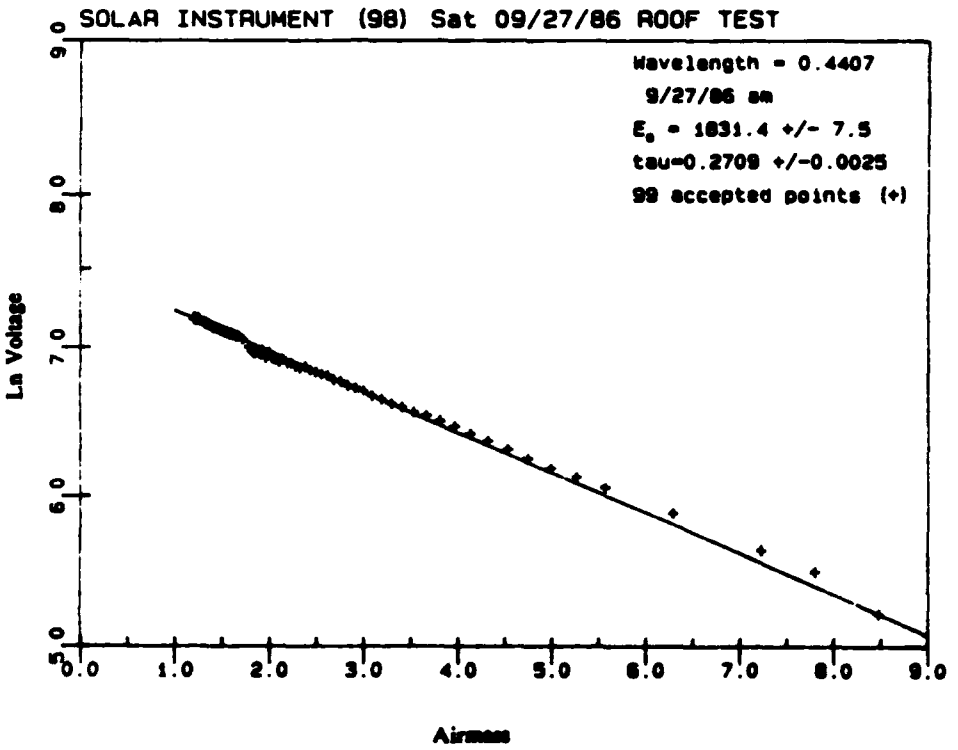

Figure 2.1 Langley-Bouguer Plot Resulting from Use of Two Lap-Top Computers

The variations in the Langley-Bouguer plots may have been due to subtle differences in aiming the instrument at the sun when the tracking program was reinitialized. Early in the morning, when the sun is near the horizon and its intensity is weak, it is difficult to ensure accurate aiming with the present sighting arrangement. This could account for possible errors in the instrument's alignment with the sun. A possibility for a new solar sight is discussed in the following section on hardware-related modifications.

In order to eliminate the need to switch lap-top computers during the middle of data collection, the data collection software was modified to write the

data to a 3.5 inch double-sided disk. This enables the Autotracker to function without interruption for over nine hours.

The solar tracking software has also been modified to use the full 22 Chebyshev coefficients found in the Almanac for Computers published by the U.S. Naval Observatory. Previously, only 11 were used. With the full 22 coefficients in use, the maximum expected computed declination error is three seconds (Almanac for Computers 1987). Using a 2° field of view, this source of tracking error is now insignificant.

The Autotracker's most significant problems arose from two sources. The first was hardware in the instrument itself and the second involved errors in calibration factors used during data reduction, errors which could indicate subtle changes in some of the instrument's optical components with time.

Hardware-Related Modifications

Detector Temperature Control. The only internal modification made to the Autotracker involved the detector mount inside the radiometer section. Both the silicon and lead sulfide detectors are held in a common sliding mount. This allows them to use common optics and filters.

To provide temperature stabilization, the detectors are heated to 48° C, which is 1.5°C higher than the highest internal temperature ever recorded within the Autotracker's radiometer. This record temperature occurred when ambient air temperature reached 46°C. Since the original design called for battery operation in the field, thermo-electric coolers were not considered feasible (Castle 1985). Even with external power sources, thermo-electric cooling might not be practical because it would have to maintain a temperature differential of 60°C below ambient for the detector slide during hot weather operation. This is near the performance limit of

applicable thermo-electric coolers. Extensive redesign of the radiometer would also be required in order to accommodate the cooler and to provide for heat dissipation.

A temperature sensor is located in the center of the detector slide. The original slide was made from aluminum with the heater element attached directly to the detectors. Monitoring of the temperature readings indicated erratic temperature stabilization, with the temperature varying as much as 3° C over the course of several hours of measurements.

A new detector slide was designed, made of copper with provision in the outer edge of the slide for a strip-heater thermofoil. This provides even heating throughout the block, and a temperature stable to ±0.1°C. Copper was chosen because it provides an increase in thermal conductivity by nearly a factor of two and a 30 percent decrease in thermal expansion compared to aluminum.

Figure 2.2 provides a dramatic illustration of the results of temperature instability on the lead sulfide detector. The seven points plotted around an airmass of three were collected while the detector was still warming to the stabilization temperature.

The lead sulfide detector is very sensitive to temperature fluctuations at all wavelengths. The silicon detector's responsivity may be susceptible to temperature fluctuations at wavelengths above 0.9 μm (Castle 1985).

Solar Tracking Stability. The Autotracker repeatedly experienced a decrease in output voltage around solar noon. This decrease was never observed in results from the Reagan instrument and so was judged not to be a true atmospheric effect. This effect is slightly noticeable in Figure 2.2 as a 'hook' around an airmass of one. The cause appeared to be variations in solar tracking. Such variations in tracking could have been due to an accuracy limitation in the tracking algorithm or to a physical problem with the platform. In addition to the update to

the tracking program already discussed, three adjustments were made to the Autotracker to eliminate this problem. An additional future modification is proposed. The first was a modification in the method used to independently adjust the level of the individual feet of the Autotracker's tripod. Acorn nuts were added to the adjustment bolts allowing fine height adjustments using a socket wrench. Also, weight distribution platforms were designed to allow the distribution of the Autotracker's weight over a larger area to prevent settling on soft surfaces. Lastly, the worm gear in the elevation turntable was tightened. It was found to be loose enough to allow movement of the turntable corresponding to an angular change in elevation in excess of 1°. Such an error would have significantly affected radiometer positioning during operation at high elevation angles.

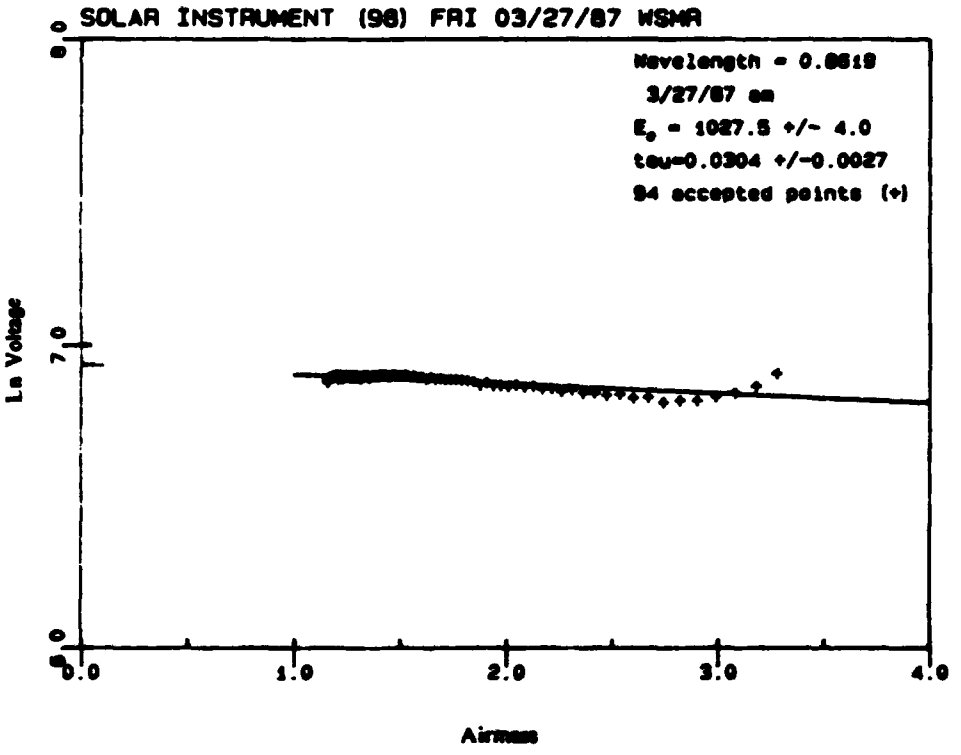

Figure 2.2 Effects of Detector Temperature Instability on Output Voltage

The proposed future modification involves a new solar sight. It is possible to use crossed linear polarizers to achieve a transmittance of a few percent in the visible. When used in conjunction with a crosshair arrangement this would allow for direct aiming at the sun during tracking program initialization. It would also provide the capability to precisely evaluate solar tracking accuracy throughout the course of data collection.

Waveplate Calibration Factors. The Autotracker is equipped with a quarter waveplate to allow calculation of the Stoke's parameters for polarization measurements. Using a camshaft design, the waveplate is placed into the beam and then retracted. This results in every other spectral band being sampled with the waveplate in position. During data reduction, a calibration factor is applied for each band to account for the transmittance of the waveplate. A number of these factors were found to be in error. In the IR bands the effect was obvious, as illustrated in Figure 2.3. Figure 2.4 is the same data, only with a correct waveplate calibration constant applied. For Bands 10, 11, and 12 the correct calibration factor had not been previously determined. A value of 1.04 had been arbitrarily assumed for each of those bands.

Because the magnitude of the error was not as great, the effects on the shorter wavelength bands was not as dramatic. In those bands the result was a slight oscillation in the points on the Langley-Bouguer plot. This problem arose because the total number of wavelength bands using both detectors is odd. Therefore, for each band, the waveplate is in the opposite position on alternating data collection cycles . The updated values of the waveplate calibration factors were determined in the laboratory using a General Electric type FEL 1000 watt lamp as the source and a 2° field of view. Data were collected using a calibration program, CAL98.BAS. This program is identical to the field data collection

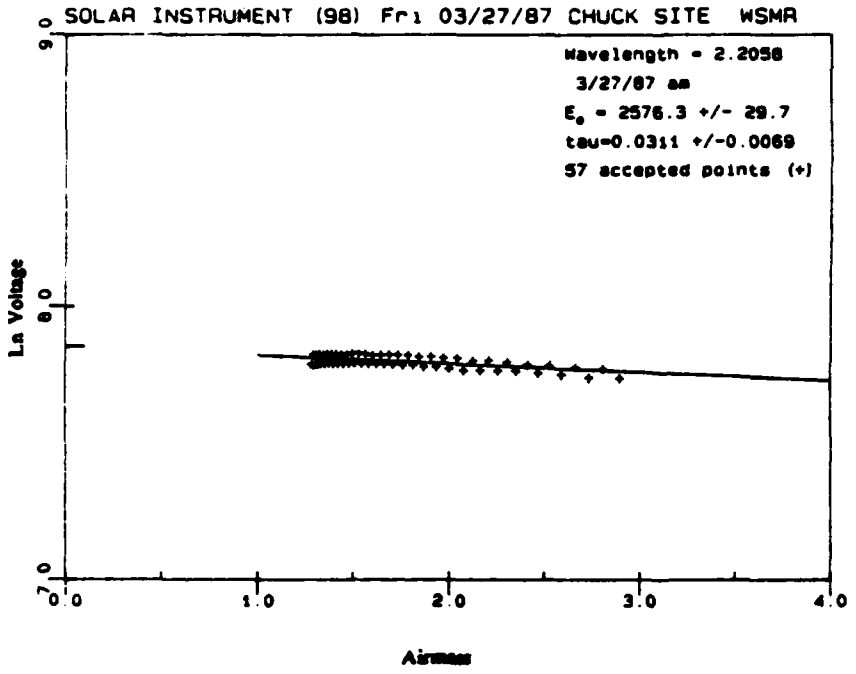

Figure 2.3 Langley-Bouguer Plot in the IR with an Incorrect Waveplate Calibration Factor Applied

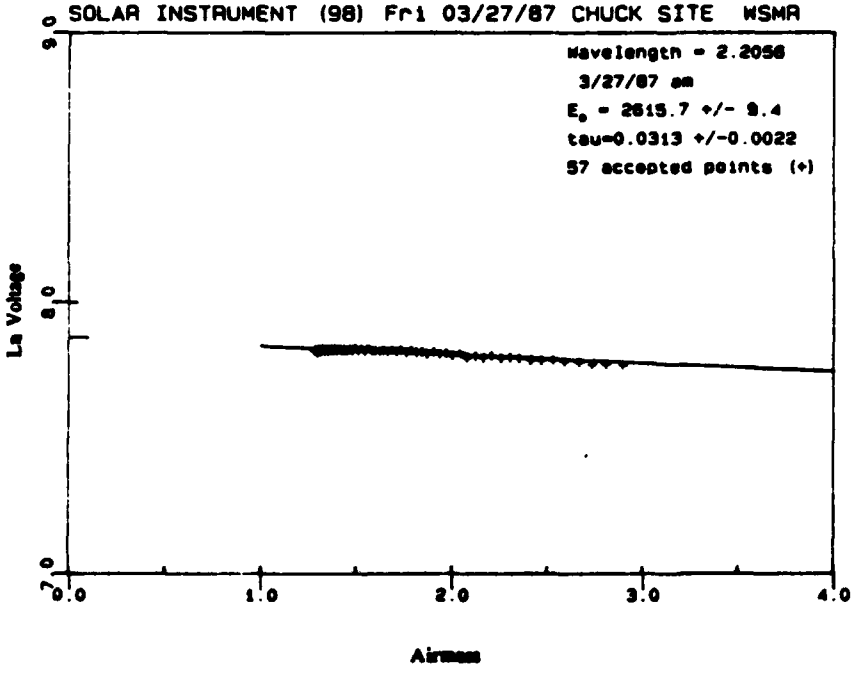

Figure 2.4 Same Data as in Figure 2.3, but Using a Corrected Waveplate Calibration Factor

program with the exception that the solar tracking algorithm is removed. Table 2.1 summarizes the changes made to the waveplate calibration factors.

Table 2.1 Summary of Waveplate Calibration Factor Changes

Band	Old Value	New Value	Change
1	1.081	1.081	0
2	1.067	1.065	-0.2
3	1.041	1.042	+0.1
4	1.021	1.019	-0.5
5	1.014	1.019	+0.5
6	1.008	1.013	+0.5
7	1.009	1.005	-0.4
8	1.006	1.014	+0.8
9	1.004	1.013	+0.9
10	1.004	1.005	+0.1
11	1.004	1.034	+3.0
12	1.004	1.048	+4.4

Neutral Density Calibration Factors. Similar in function to the waveplate calibration factors are the neutral density calibration factors which allow data collected using different neutral density filters to be properly compared. The neutral density calibration factors are relative values with neutral density filter 1, which is ordinary glass, assigned a value of 1.

The neutral density filter selection is an automatic feature of the data collection program. The computer makes the selection so that the digital detector output counts remain between 200 and 4095.

Neutral density calibration factors were found to be in error in Bands 1, 2, 4, 5 and 8. The amount of the error varied from 11 percent to 21 percent, inversely proportional to wavelength.

The manner in which this error manifested itself is illustrated in Figure 2.5. The discontinuity in the Langley-Bouguer plot corresponds exactly to a change in neutral density filter. The errors were such that in Bands 1 and 2, the slopes of

the Langley-Bouguer plots were reduced. However, in Bands 4, 5 and 8 the slope would have been increased, as shown in Figure 2.5 for Band 4. This particular error in Band 4 had a direct impact on the current method of ozone determination, discussed in Chapter 3.

The neutral density calibration factors in error were readily identified by analyzing available Langley-Bouguer plots. Corrected values were calculated by determining the ratio of the intercepts of Langley-Bouguer plots created for the separate line segments defined by the change in neutral density filter selection. Laboratory measurements were not used due to the large dynamic range required of the source. Figure 2.6 is a Langley-Bouguer plot of the same data as Figure 2.5, only using a more accurate value for the applicable neutral density calibration factor. Note that the optical depth determined from the Langley-Bouguer plot in this example was reduced by 32 percent.

In summary, Figures 2.7 and 2.8 illustrate the result of these corrections and modifications to the Autotracker. Figure 2.7 is a comparison of the optical depths determined using the Autotracker to those determined using the Reagan instrument on 14 October 1986. At that time, none of the changes discussed here had been implemented. The Autotracker data are represented by squares and the Reagan instrument data by crosses. In sharp contrast are the results shown in Figure 2.8. This graph is a comparison between the Autotracker and two versions of the Reagan solar radiometer on 14 September 1987. The Autotracker data are again represented by squares. Improvement in Autotracker performance is evident. Some inconsistencies remain in the region around 0.6 μm. It is important to note that an additional spectral band centered at 0.94 μm was added to the Reagan instrument between these two dates.

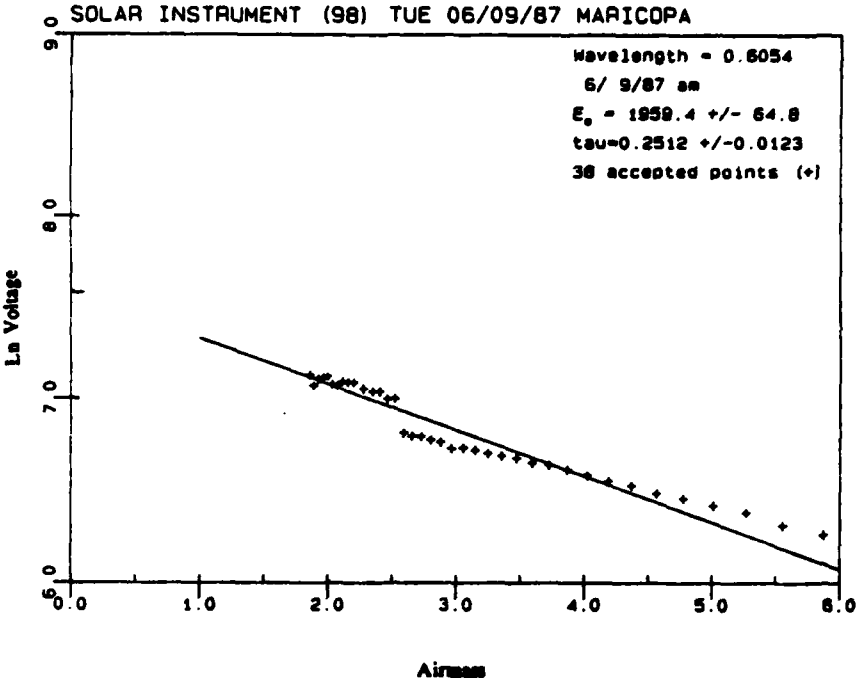

Figure 2.5 Langley-Bouguer Plot Generated Using an Incorrect Neutral Density Calibration Factor

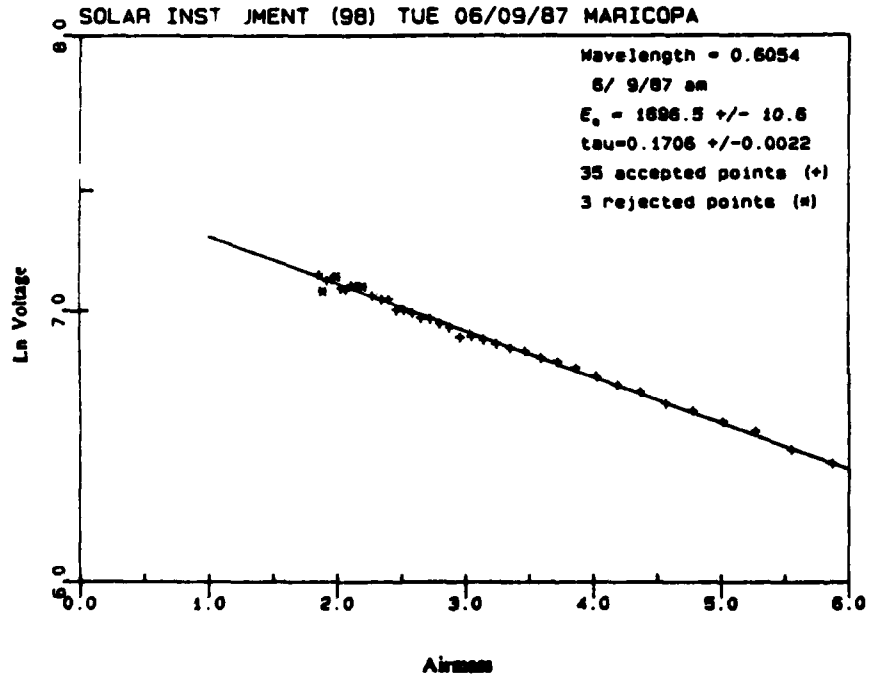

Figure 2.6 Same Data as in Figure 2.5, but Using an Updated Value for the Neutral Density Calibration Factor

Even when the collected data are free from instrument errors, there are limitations on how accurately optical depths can be computed using it.

Optical Depth Calculation Considerations

Langley-Bouguer Plot Technique Limitations

The Langley-Bouguer technique, described in Chapter 1, has some limitations which must be considered in both the context of routine data reduction and in the long-term goal of radiometer calibration.

Data Reduction Considerations. Routine data reduction is important because in attempts to radiometrically calibrate satellites an accurate determination of optical depth is of great importance. Calculation of the solar constant is of use as a check of instrument performance.

The ideal Langley-Bouguer plot is perfectly linear. The effects of actual conditions, though, may result in an erratic plot in which the points are not collinear. The cause of erratic data may be instrument or atmosphere related. Figure 2.2 is an excellent illustration of instrument-related inaccuracies resulting in an obviously incorrect value for the slope. In addition to systematic errors such as these, an occasional isolated erroneous measurement will be recorded. Such points may be caused by high cirrus partially obscuring the sun or intermittent, non-repeatable, instrument malfunctions. It is important that all suspect points, with the error due to identifiable causes, be removed. Table 2.2 contains optical depth results from data collected on 27 March 1987, first with all collected data included and then with identifiably erroneous data removed. The percentage change at the longer wavelengths is dramatic.

Slight variations in surface irradiance due to small changes in optical depth are often experienced. It is well-established (Shaw et al. 1972) that under

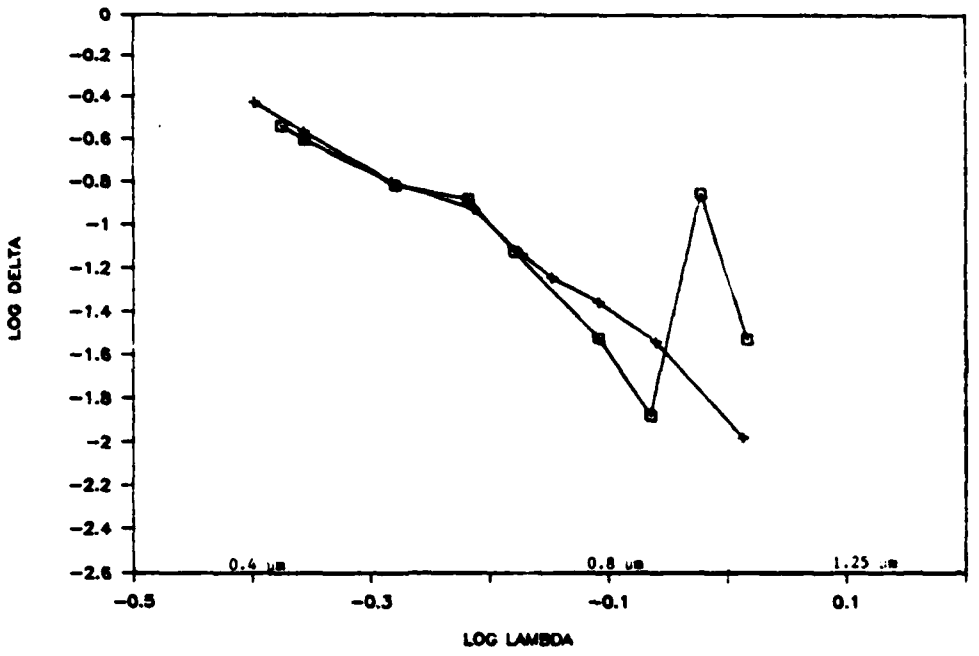

Figure 2.7 Comparison of Autotracker (□) and Reagan Solar Radiometer (+) Optical Depths for 14 October 1986

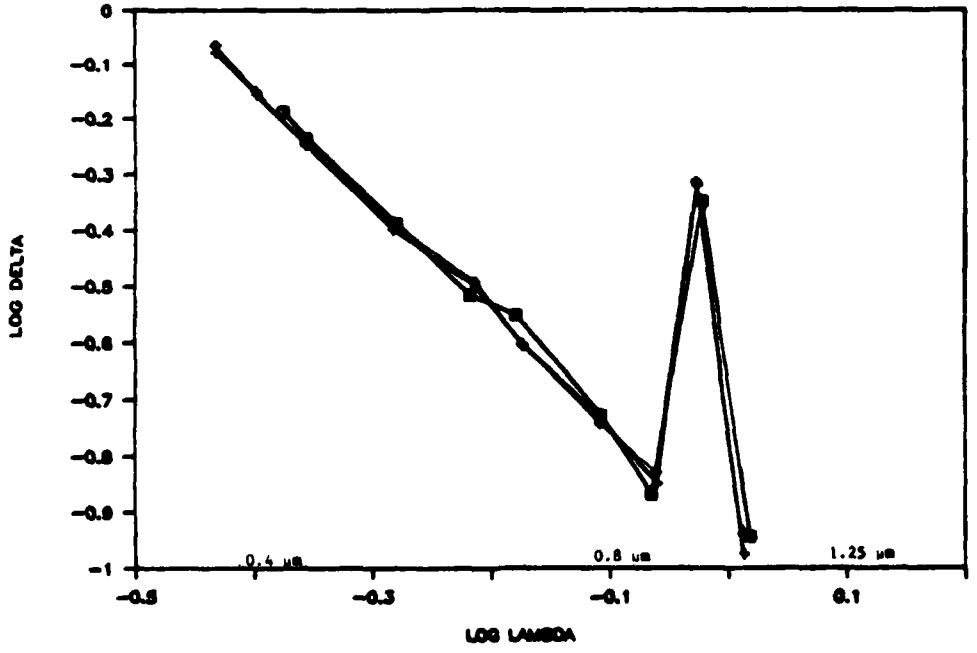

Figure 2.8 Comparison of Autotracker (□) and Reagan Solar Radiometer (◇, +) Optical Depths on 14 September 1987

otherwise favorable conditions a least squares fit yields an accurate determination of slope and intercept values in these cases.

Table 2.2 Comparison of Optical Depths Determined Using All Data Collected Versus Properly Screened Data

$\lambda(\mu m)$	$\delta \rightarrow$All Data Included	$\delta \rightarrow$Screened Data
0.4214	0.3434	0.3484
0.6054	0.2188	0.2229
0.8619	0.0532	0.0732
2.2058	0.0173	0.0311

The basic premise of the Langley-Bouguer technique is that the optical depth remains constant over the course of the measurements. If the optical depth is varying fairly continuously the result should be a non-linear Langley-Bouguer plot. Under these conditions the technique is obviously invalid. However, it has been shown (Reagan et al. 1984) that if the change in optical depth meets certain insidious systematic conditions the result is a straight line Langley-Bouguer plot, but with incorrect values for slope and intercept. In either case, accurate optical depth determination for specific times is still possible if the instrument in question is properly calibrated.

Instrument Calibration Considerations. An instrument of this type is calibrated if the relationship between its output and the exoatmospheric solar irradiance is known and measurements are repeatable. An established method of calibration is to use the Langley-Bouguer technique on measurements made at high elevations, where the effects of atmospheric variability are minimized.

It is of interest to examine the intercept history of both the Autotracker and the Reagan instrument over a period of one year. Figure 2.9 is a plot of

intercept values corrected for the mean earth-sun distance for both instruments at 0.44 μm normalized to the intercept value on 27 March 1987. The graph includes data from seven satellite calibration dates from October 1986 to June 1987. The Autotracker intercepts are represented by squares and the Reagan instrument intercepts by crosses. The Reagan instrument values exhibit a slight decrease over this time period while those of the Autotracker show considerable variation. This result justifies higher confidence in the results obtained using the Reagan solar radiometer.

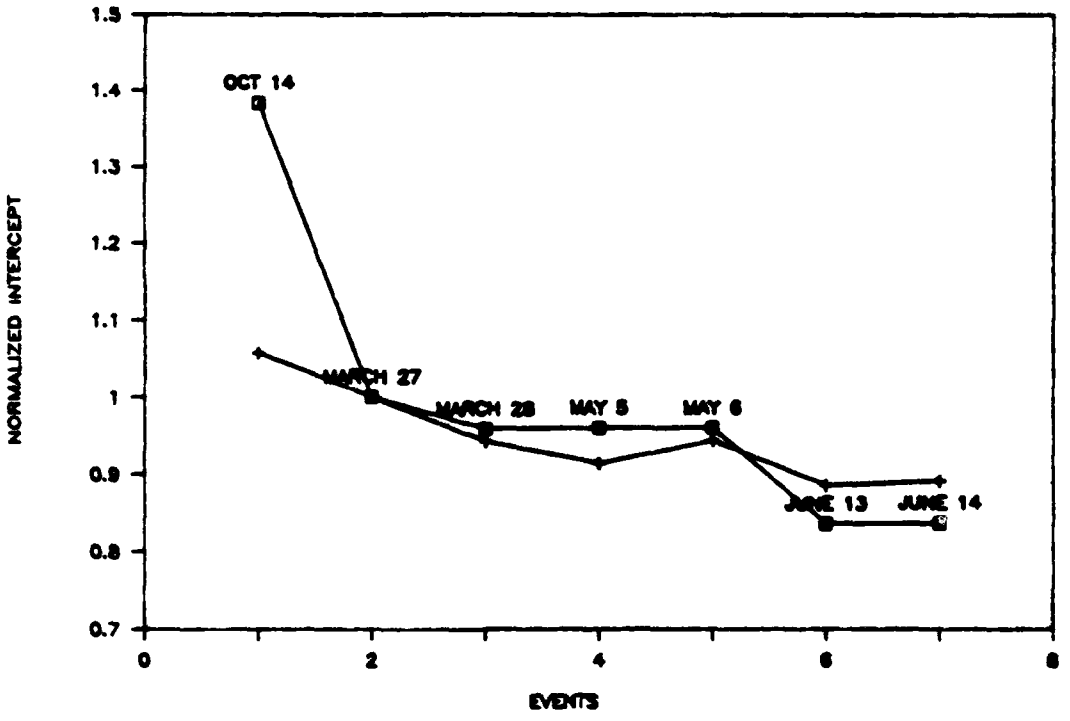

Figure 2.9 Comparison of Normalized Intercept Values for the Autotracker (□) and Reagan Solar Radiometer (+) at 0.44 μm

If the instrument's intercept value for a given spectral band is well established, then an instantaneous value for optical depth corresponding to an individual measurement on a given day can be computed (Shaw et al. 1972). This

instantaneous value represents the slope of a line drawn through the established point of intercept and the point in question. This instantaneous value is the actual optical depth existing at that time. An accurate calibration is therefore extremely valuable. Certain factors must be taken into account when attempting to calibrate an instrument as outlined by Reagan et al. (1986). One such factor includes limiting the airmass to a value of six or less which would eliminate the complexities of a spherical atmosphere. It is also necessary to limit bandwidths to 10 nm in the visible spectrum in order to avoid errors due to the monochromatic nature of Beer's Law. The maximum allowable bandwidth approaches 1 μm in the near IR (Thomason et al. 1982). The Autotracker meets these bandwidth conditions, as shown in Table 1.1. The last major factor to be considered here is the contribution of diffuse radiation scattered into the instrument's field of view. This correction is discussed in the next section.

Corrections to Total Optical Depth

During the course of this work it was found that values for total optical depth could be corrected for both temperature fluctuations of the detector and for the contribution of diffuse radiation scattered by aerosols into the instrument's field of view.

Correction for Detector Temperature Fluctuation. To a limited extent it appears possible to retrieve a corrected value for optical depth from measurements taken while the temperature of the detector is fluctuating. The case discussed here involves the Reagan instrument's spectral band at 1.03 μm and is intended as an example of the correction process.

The response of a silicon detector should be insensitive to temperature changes out to a wavelength of approximately 0.9 μm. Beyond that, temperature fluctuations can have a significant effect on its response (Castle 1985).

The Reagan instrument's silicon detector is normally stabilized at 39° C. During cold (2°C), windy (15 mph) conditions at White Sands, New Mexico on 28 March 1987 the heater element required three hours to stabilize the detector at this temperature. The optical depth calculated at 1.03 μm from the original roughly linear Langley-Bouguer plot was 0.0876. This appeared too high when compared to the optical depths computed for shorter wavelengths. Using a value for change in responsivity with temperature of 0.5 percent per degree Celsius (Reagan 1987), the data were corrected. The resulting roughly linear Langley-Bouguer plot had a slope of 0.0674, a change of 23 percent. This new value appeared more reasonable. A similar correction was made for data taken when the detector's temperature climbed above 39° C and the resulting optical depth also appeared more reasonable than the original value.

Correction for the Contribution of Diffuse Radiation. Due to the fact that the fields of view of the instruments used in data collection are larger than the 0.5° subtended by the sun, there will be a contribution to the power incident on the detector from diffuse radiation scattered by aerosols into the instrument's field of view. If gaseous absorption is also present, this can be expressed mathematically as,

$$\Phi = E_o t_g e^{-m(\delta Ray + \delta Mie)} + \Phi_d \qquad (2.1)$$

where Φ is the measured flux,

t_g is the gaseous transmittance,

Φ_d is the diffuse flux.

The diffuse flux can in turn be expressed by,

$$\Phi_d = \int_\Omega L(\delta,\mu,\mu_s,\phi,\phi_s)\cos(\theta-\theta_s)\,d\Omega \qquad (2.2)$$

where Ω is the instrument's field of view,

and $L(\delta,\mu,\mu_s,\phi,\phi_s)$ is the downward radiance.

The s subscripts refer to the direct solar beam. Since $\theta \cong \theta_s$ in the case of forward scattering, then $\cos(\theta - \theta_s) \cong 1$. The downward radiance can be expressed in the single scattering approximation as,

$$L(\delta,\mu,\mu_s,\phi,\phi_s) \cong \frac{E_o}{4\pi\mu}\, e^{-(\delta_{Ray}+\delta_{Mie})/\mu}\,(\delta_{Ray}P_{Ray}(\theta) + \delta_{Mie}P_{Mie}(\theta)) \quad . \qquad (2.3)$$

Now the scattering phase function $p(\theta)$ is defined by,

$$p(\theta) = \frac{\delta_{Ray}\ P_{Ray}(\theta) + \delta_{Mie}\ P_{Mie}(\theta)}{\delta_{Ray} + \delta_{Mie}} \quad . \qquad (2.4)$$

With $\mu \cong \mu_s$ for the case of forward scattering, equation (2.2) can now be written,

$$\Phi_d \cong \left[\frac{E_o}{4\pi\mu_s}\right] e^{-(\delta_{Ray}\ +\ \delta_{Mie})/\mu}\,(\delta_{Ray} + \delta_{Mie}) \int_\Omega p(\theta)\,d\Omega \quad . \qquad (2.5)$$

Due to the symmetry of the phase function in azimuth, we can write,

$$\int_\Omega p(\Theta)\,d\Omega = \int_0^{2\pi}\int_{\cos\Omega}^{1} p(\cos\Theta)\,d\cos\Theta\,d\phi = 2\pi\int_{\cos\Omega}^{1} p(\mu)\,d\mu = 2\pi A \quad . \qquad (2.6)$$

Equation (2.5) now becomes,

$$\Phi_d \cong \left[\frac{E_o}{4\pi\mu_s}\right] e^{-(\delta_{Ray}\ +\ \delta_{Mie})/\mu_s}\,(\delta_{Ray} + \delta_{Mie})\,(2\pi A) \quad . \qquad (2.7)$$

Rearranging terms in equation (2.7) results in,

$$\Phi_d \cong E_o\, e^{-m(\delta_{Ray}\ +\ \delta_{Mie})}\,(\delta_{Ray} + \delta_{Mie})\left[\frac{A}{2\mu_s}\right] \quad . \qquad (2.8)$$

Now, if t_g is assumed equal to one, equation (2.1) can be rewritten as,

$$\Phi \cong E_o \, e^{-m(\delta_{Ray} + \delta_{Mie})} \left[1 + \frac{A(\delta_{Ray} + \delta_{Mie})}{2\mu_s}\right] . \qquad (2.9)$$

In a first order approximation based on $\left[\frac{A(\delta_{Ray} + \delta_{Mie})}{2\mu_s}\right] << 1$, equation (2.9) becomes,

$$\Phi \cong E_o \, e^{-m(\delta_{Ray} + \delta_{Mie})} \, e^{A(\delta_{Ray} + \delta_{Mie})/2\mu_s} . \qquad (2.10)$$

Combining terms in equation (2.10) yields,

$$\Phi \cong E_o \, e^{-m(\delta_{Ray} + \delta_{Mie})(1 - A/2)} . \qquad (2.11)$$

So the optical depth obtained from the Langley-Bouguer plot, δ^*, can be expressed by,

$$\delta^* \cong (\delta_{Ray} + \delta_{Mie})\left[1 - \frac{A}{2}\right] . \qquad (2.12)$$

The factor (A) becomes a correction factor. The factor (A) can be computed and is a function of the value for the Junge size distribution, the field of view and wavelength involved.

The Fortran program TAUCM found in Appendix A computes this correction factor for optical depths determined from a Langley-Bouguer plot. Figure 2.10 is an illustration of the magnitude of the correction term 1/(1 - A/2) in terms of wavelength and field of view, assuming a Junge size distribution of 3.0. For a radiometer with a FOV of 2°, it can be seen from Figure 2.10 that the amount of correction is on the order of one percent for the wavelengths of interest in this study.

Table 2.3 contains the percentage change in optical depth at selected wavelengths for three different Junge slopes encountered during satellite calibration

field work. The table illustrates the marked increase in forward scattering encountered when a predominance of large particles is present as indicated by the lower value for ν. The Autotracker's 2° FOV was used for these calculations. The diffuse radiation correction is somewhat greater for Reagan instrument optical depths due to its larger FOV.

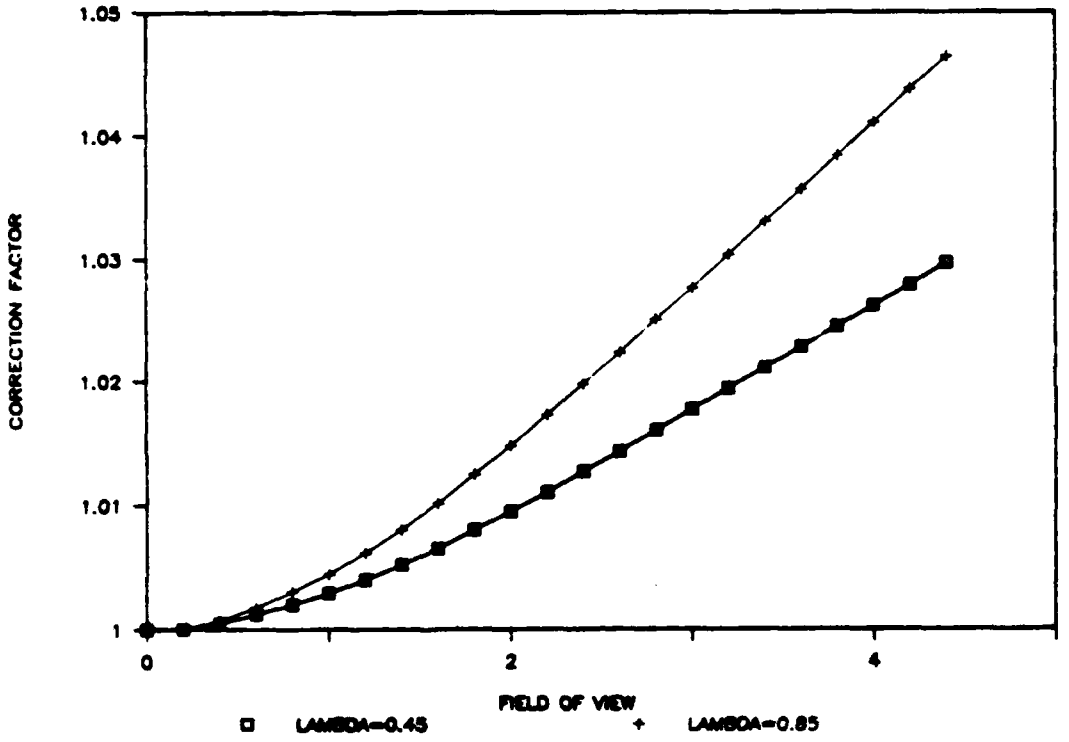

Figure 2.10 Effect of Changes in Wavelength and Field of View on the Correction to Optical Depth Required Due to the Contribution of Diffuse Radiation

Table 2.3 Percentage Change in Optical Depths due to the Correction for the Contribution of Diffuse Radiation for Three Values of ν

	Junge Size Distribution (ν)		
$\lambda(\mu m)$	2.49	3.17	3.65
0.4214	1.04	0.40	0.18
0.6054	1.5	0.46	0.18
0.8619	3.39	0.81	0.44

While the absolute value of the correction is greater at shorter wavelengths, the percentage change increases with wavelength. This results from the decreasing contribution of Rayleigh scattering with increasing wavelength. Under most conditions, the magnitude of this correction to optical depth will be on the order of one percent or less.

Once accurate values for total optical depth are established using a solar radiometer, it is then possible to determine the amount of attenuation taking place due to gaseous absorption. Knowing the amount of attenuation due to gaseous absorption is important for an accurate solution to a radiative transfer code and therefore important to accurate satellite radiometric calibration.

CHAPTER 3

GASEOUS CONTENT DETERMINATION

The most important gaseous absorbers in the solar reflective spectrum that pertain to the calibration of TM, SPOT and AVHRR are ozone and water vapor due both to their level of absorption and the variability of their concentrations in the atmosphere. The current techniques for determining the amount of each present in the atmosphere at satellite overpass times are discussed in this chapter. The estimated accuracy of these calculations is also examined. Figures 3.1 - 3.4 are included at this point to illustrate representative spectral transmittance characteristics of each of the four gaseous absorbers having the greatest effect on satellite calibration work. Oxygen and carbon dioxide are uniformly mixed gases and can be seen to have only a limited effect at most wavelengths. Additionally, since they are uniformly mixed gasses, the total amount of each present in the atmosphere depends only on atmospheric pressure, a quantity accurately known. These figures are extracted from Tanre' et. al. (1986). Also see Table 5.1 for representative transmittance values in specific satellite bands.

Ozone

To accurately calibrate TM2, the SPOT High Resolution Visible (HRV) 1 and Panchromatic Band and AVHRR Band 1 it is necessary to determine the actual amount of ozone present in the atmosphere during calibration data collection. Ozone content has been found to vary fairly predictably during the course of the year. The pattern of the variation is basically sinusoidal with the minimum and maximum values dependent on the latitude of the observer. Figure 3.5 is an

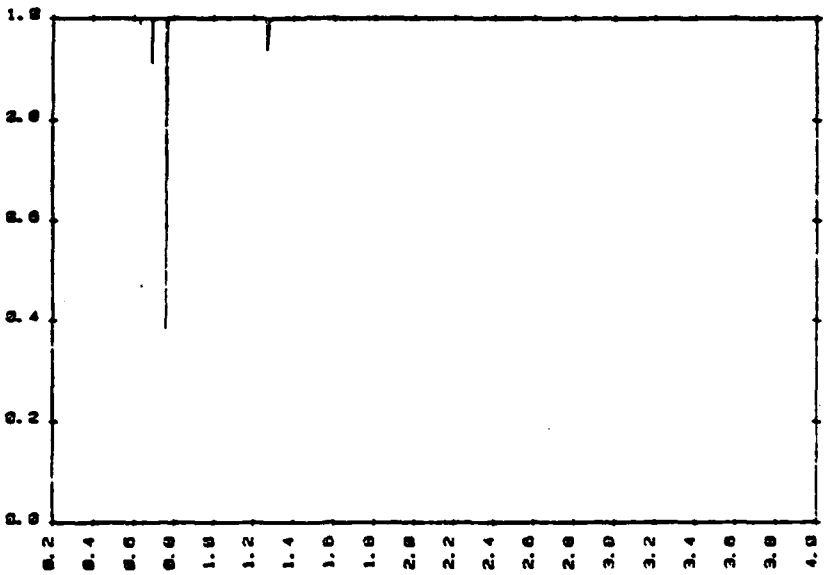

Figure 3.1 Spectral Transmittance of Oxygen (O_2)

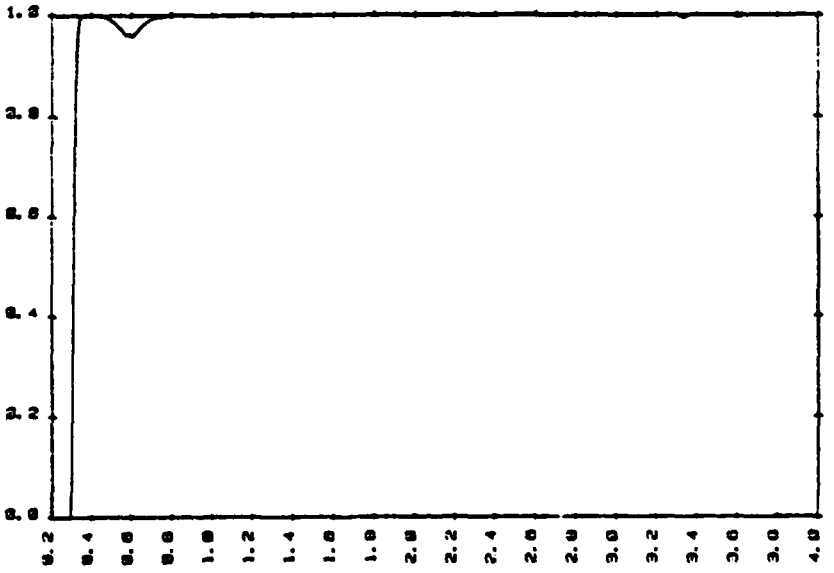

Figure 3.2 Spectral Transmittance of Ozone (O_3)

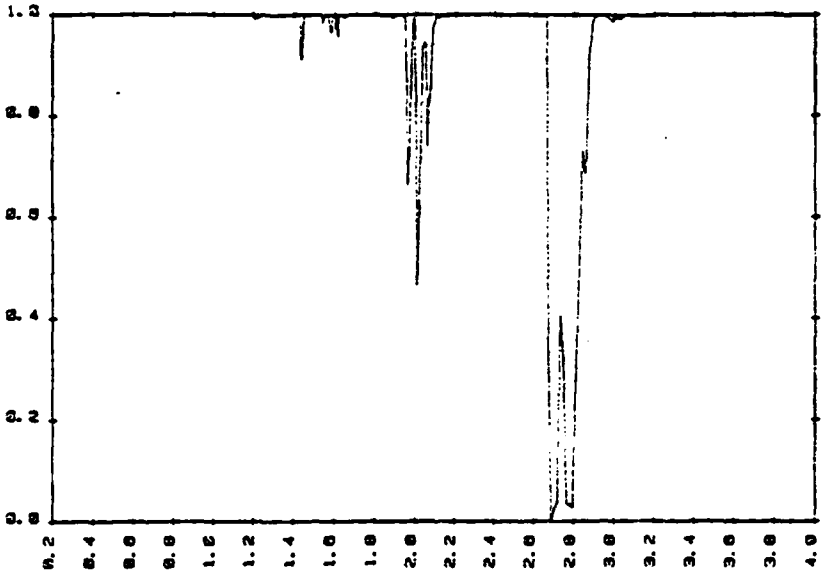

Figure 3.3 Spectral Transmittance of Carbon Dioxide (CO_2)

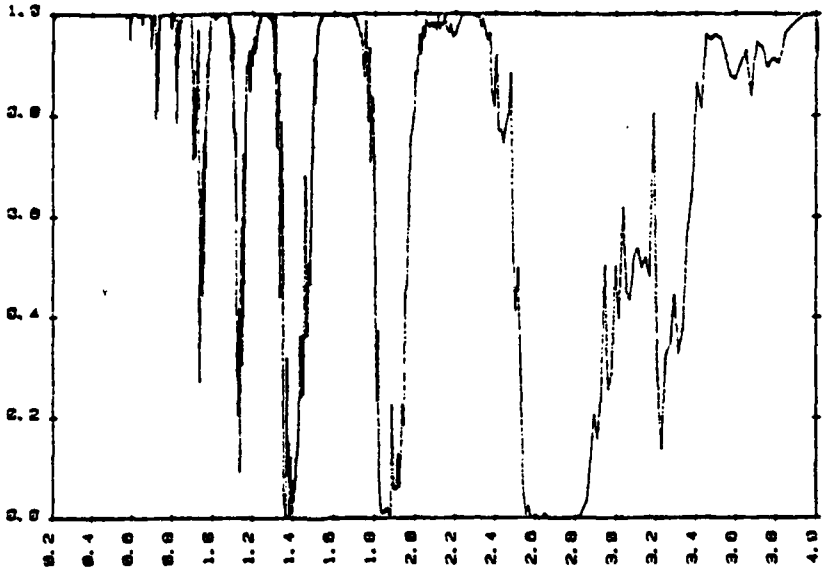

Figure 3.4 Spectral Transmittance of Water Vapor (H_2O)

illustration of the seasonal change in ozone content relative to the latitude of the observer. Local anomalies in this pattern are possible.

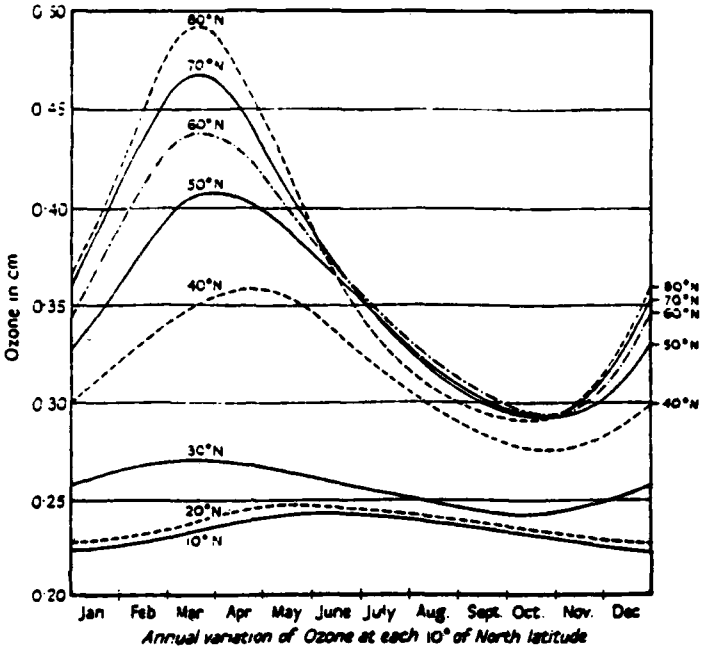

Figure 3.5 Ozone Content Variation with Latitude and Season, Dobson (1963)

Current Method of Ozone Determination

A value for the atmospheric ozone content can be calculated based on optical depths determined using the Langley-Bouguer technique. The method centers on the optical depth for a spectral band around 0.6 μm in the middle of the broad Chappuis ozone absorption band. For these calculations the Autotracker and the Reagan instrument spectral bands at 0.61 μm are used. The total optical depth at this wavelength is the sum of components due to molecular scattering, aerosol optical depth and ozone absorption.

Assuming atmospheric pressure is accurately known, the Rayleigh optical depth approximation is computed using equation (1.4). The aerosol optical depth is determined by computing the Ångström wavelength exponent (α) as outlined in Chapter 1. Once the wavelength exponent is known, the theoretical aerosol optical depth for the wavelength near 0.6 μm can be computed. The computed aerosol optical depth will be correct if the aerosols closely follow a Junge size distribution. The validity of this assumption in many cases is questionable. Analyses in the past have shown that strictly Junge type distributions occur only 20 percent of the time in the Tucson area (King et al. 1978).

Once the Rayleigh and Mie components of optical depth are known, their sum is subtracted from the total optical depth. The remainder is the optical depth due to ozone absorption. The actual quantity of ozone present is then found using the relation,

$$\delta_{OZ}(0,\lambda) = N_{OZ}\sigma_{OZ}(\lambda) \qquad (3.1)$$

where $\delta_{OZ}(0,\lambda)$ is the ozone optical depth measured at ground level, N_{OZ} is the atmospheric ozone content and σ_{OZ} is the ozone absorption coefficient for the wavelength in question (Kastner 1985). Values for σ_{OZ} have been experimentally determined by Vigroux and others. A table listing these values is found in Iqbal, p. 127. Ozone content is usually expressed in units of atm-cm. A value of one atm-cm would indicate that if all the atmospheric ozone in a vertical column one centimeter on a side were condensed at standard pressure and temperature the result would be a column one centimeter high.

Because ozone absorption is weak in the Chappuis band, any error in determination of either the total or Mie optical depths will result in erroneous values of ozone content using this method. The impact on these calculations of the

error in the Autotracker's Band 4 neutral density calibration factor, discussed in Chapter 2, is obvious.

There are several sources of information on ozone content which can be used to verify the results of the method just described. The first source is an expression developed by King and Byrne (1976) which determines a seasonal value for ozone content over Tucson. Because the latitude of the various calibration sites is approximately equal to Tucson's, this expression can be applied for them as well. The expression, which yields a value in atm-cm, is,

$$N_{OZ} = 255.3 \pm 4.0 + (42.6 \pm 5)\sin(2\pi x - \phi) \qquad (3.2)$$

where x is the fractional time of the year,

and ϕ determines the time of peak distribution.

A second source is the direct measurement of atmospheric ozone content at Boulder, Colorado and Fresno, California by NOAA's Environmental Research Laboratory. These measurements, if made under clear skies, are considered accurate to two percent (Grass 1987). These values have been corrected for the difference in latitude between their point of measurement and the satellite calibration sites.

Also considered are values for ozone content from the work of London et al. (1976), an analysis of average world atmospheric ozone content. Table 3.1 contains values for ozone content from the above sources for five days of satellite calibration measurements during 1987. The Autotracker results are obviously in error for the first three days. These errors are attributed to instrument malfunctions involving possible vignetting in some of its spectral bands unrelated to the neutral density calibration factor error.

Based on the values directly measured, the actual ozone content during the spring appears to be 10 percent to 20 percent higher than predicted by

historical data. During the summer there is a good correlation between the predicted and directly measured values. These results indicate that under most conditions it is possible to compute an ozone content accurate to approximately 10 percent using the current method. The affect of this uncertainty on satellite calibration work will be assessed in Chapter 5.

Table 3.1 Comparison of Values for Ozone Content Obtained from Five Independent Sources

	27 March	6 May	9 June	13 June	14 June
Autotracker	0.714	0.561	0.468	0.328	0.322
Reagan Instrument	0.367	0.348	N/A	0.360	0.374
Measured Value	0.373	0.335	0.304	0.292	0.292
Seasonal Values	0.302	0.306	0.292	0.290	0.290
London et al.	0.308	0.304	0.286	0.286	0.286

Alternate Method of Ozone Determination

It may be possible to achieve a more accurate ozone content determination by working in another part of the spectrum. Presently, a spectral band in the Chappuis absorption band must be used to compute total ozone content because of the optics used in the Autotracker. It would be preferable to work in the very strong Hartley absorption band in the ultraviolet (UV). However, this is not possible with the Autotracker because the transmittance of optical glass falls rapidly to zero at wavelengths shorter than 0.38 μm (Smith 1966 p.154). Table 3.2 lists the results of an analysis for possible measurements in the UV. The calculations assume as representative values: standard atmospheric pressure, an airmass of three, an ozone content of 0.250 atm-cm and an aerosol optical depth based on a visibility of 23 km for an Ångström wavelength exponent of one. In this table R(Si) is the typical response of a silicon detector. The bottom row is the

relative output at each wavelength normalized with respect to that at 0.4 μm. These results indicate measurements might be practical at wavelengths as short as 0.32 μm. Measurements of this type would require a new portable instrument with a single spectral filter using imaging optics made from sapphire or some other suitable UV-transmitting glass (Handbook of Optics 1978, p.7-23).

Table 3.2 Analysis for Ozone Measurements in the UV

λ (μm):	0.31	0.32	0.33	0.40
δ_{O_3}	2.617	0.724	0.192	0
δ_{Ray}	1.092	0.958	0.844	0.345
δ_{Mie}	0.323	0.313	0.303	0.250
δ_T	4.032	1.995	1.339	0.595
$e^{-3\delta T}$	$6x10^{-6}$	0.0025	0.018	0.167
E_o (W/m²/μm)	581	730	926	1614
R(Si)	0.013	0.018	0.022	0.11
$RE_o e^{-3\delta T}$	$4x10^{-6}$	0.033	0.37	30
Normalized	10^{-6}	10^{-3}	0.012	1

Water Vapor

Calibration of Thematic Mapper Bands 4, 5, and 7, the SPOT HRV 2, and AVHRR requires an accurate determination of the integrated atmospheric water vapor content. Water vapor content can be calculated from measurements of temperature and relative humidity. These measurements can either be limited only to the surface or taken in a vertical profile by a radiosonde. A value for water vapor content can also be computed using data collected in the Autotracker's spectral band centered at 0.95 μm.

Relative Humidity and Temperature Measurements

The most accurate determination of integrated water vapor content readily available comes from data collected by a radiosonde. Such measurements are typically made from the surface to the tropopause. Temperature and relative humidity measurements restricted to the surface are also made throughout the time of satellite calibration data collection. From these surface measurements a value for integrated water vapor content can be inferred by assuming a standard profile for the vertical distribution of water vapor.

Radiosonde Measurements. It is possible to compute the integrated atmospheric water vapor content using measurements made with a radiosonde. A BASIC program to used for this purpose is found in Appendix A, entitled WATER.BAS.

The radiosonde represents the only source of information readily available which allows the calculation of the vertical distribution of water vapor in the atmosphere and, correspondingly, the integrated atmospheric water vapor content. Unfortunately, the number of ground weather stations which currently launch radiosondes is very limited. However, data are available for Tucson from balloons launched from the Tucson International Airport; for White Sands, New Mexico from balloons launched at the White Sands Army Missile Base and for Mojave, California from balloons sent aloft at Edwards Air Force Base (AFB), California.

The accuracy of the value for total integrated water vapor content derived from the radiosonde data is considered to be 10 percent. This value is based on radiosonde individual measurement tolerances found in the Federal Meteorological Handbook No. 3, 1969.

The method used in WATER.BAS to calculate total atmospheric water vapor content requires the following inputs: the height of each observation in

meters above sea level and the temperature and dewpoint depression comprising that observation. Dewpoint temperature is then computed and used in conjunction with the actual temperature to compute fractional relative humidity at that height. The expression used for this calculation is based on the Clausius-Clapeyron equation and was provided by the U.S. National Weather Service at the Tucson International Airport. The value for the saturation vapor pressure of water at that height is found by interpolating from a table containing saturation vapor pressures of water for temperatures from -75°C to +50°C. The value of saturation vapor pressure depends solely on temperature. (Hipps 1987). For temperatures below 0°C the table actually contains values for saturation vapor pressure over ice. The table of saturation vapor pressures was extracted from the Smithsonian Meteorological Tables (1951).

The partial pressure of water is easily found given the saturation vapor pressure, the independently calculated value of fractional relative humidity, and the relationship that relative humidity is equal to the ratio of the partial pressure of water and the saturation vapor pressure of water. Now, the ideal gas equation,

$$P = \rho RT \tag{3.3}$$

can be used to compute water vapor density. In equation (3.3) R is the gas constant for water, which is the ideal gas constant divided by the molecular weight of water, T is temperature in degrees Kelvin, and P is the partial pressure of water at each level. The ideal gas equation is solved for the water vapor density in g/cm^3 at each incremental elevation.

To find the total integrated water vapor content, these values of density at individual observation heights are integrated over height using the trapezoid rule. If usable radiosonde data ceases prior to 12000 meters above mean sea level, water vapor extinction is assumed to occur at a height of 12000 meters and an

extrapolation is made to a value of zero at that height. Usable radiosonde data usually cease at an altitude corresponding to a temperature of approximately -40°C. At temperatures below -40°C the amount of water the air can hold is very small, typical integrated values above that level being on the order of 0.03 g/cm². Figure 3.6 is an example of the output curve of the program and is an excellent illustration of the exponential drop-off of water vapor content with height. This figure contains radiosonde data collected on 14 September 1987 at Edwards AFB, California. The results of WATER.BAS were compared to those of a similar program developed by the Department of Atmospheric Physics, the University of Arizona. The results agreed within one percent, verifying the technique used in WATER.BAS.

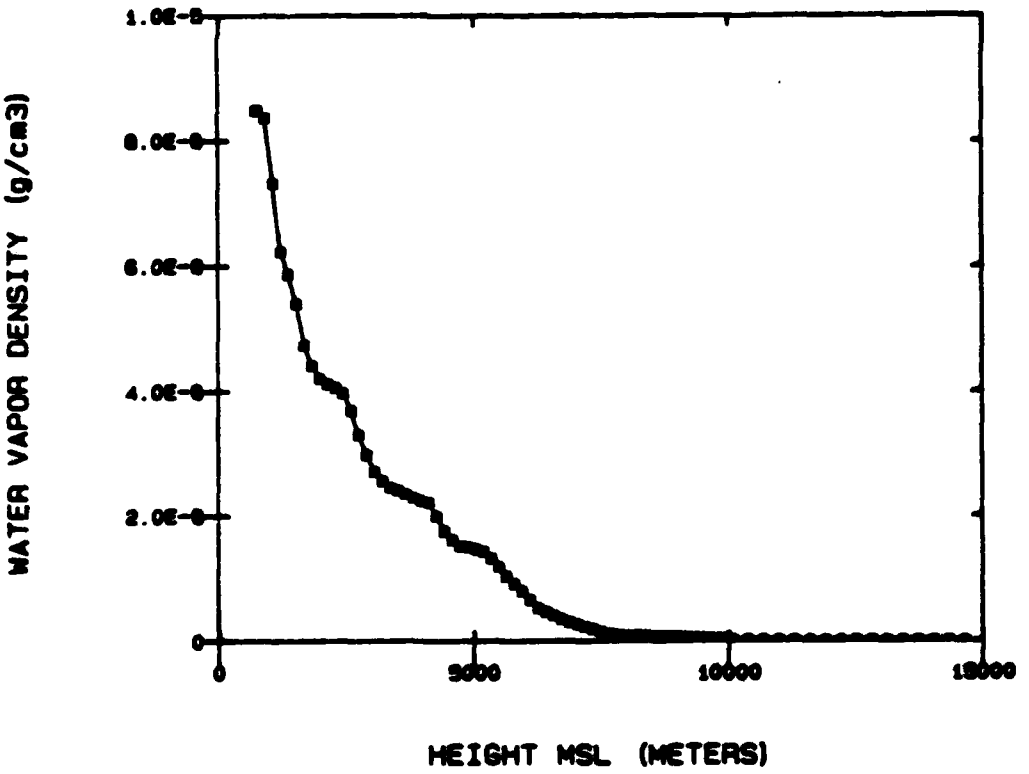

Figure 3.6 Vertical Atmospheric Water Vapor Distribution Obtained from Radiosonde Data

Ground-based Measurements. During the period of time optical depth measurements are made, surface barometric data are recorded by the Remote Sensing Group. The data collected include the time of acquisition, temperature, atmospheric pressure and relative humidity. Two other sources for this type of data are measurements made by the U.S. Air Force and measurements made by the U.S. Department of Agriculture's Water Conservation Laboratory (WCL). WCL personnel participate in each satellite calibration campaign and Air Force data are available for calibration efforts at White Sands, New Mexico and Edwards AFB, California.

Using a program similar in concept to WATER.BAS, surface data from these three sources can be used to compute the variation in surface water vapor density with time. Figure 3.7 is a comparison of results from the three sources on 5 May 1987 at Edwards AFB, California. Along the Y-axis, the Air Force results are the highest, followed by the RSG and WCL results. The WCL results are very time limited for this date. The differences between the three throughout the day are significant when considering their use to estimate integrated water vapor content. The Air Force measurements are made only once per hour which increases the effect of any inaccurate measurement. The WCL station samples every five seconds and its results indicate the rapid fluctuations possible in surface conditions.

The variation of surface water vapor density with time is the only information currently available to judge the stability of the atmospheric water vapor content. The reliability of such a judgment is unknown at this time. Knowledge of the degree of stability will be important to the water vapor content calculation involving the Autotracker's Band 8. It is important to note here that any error in the measurement of relative humidity translates into the same percentage error in the computed surface water vapor density.

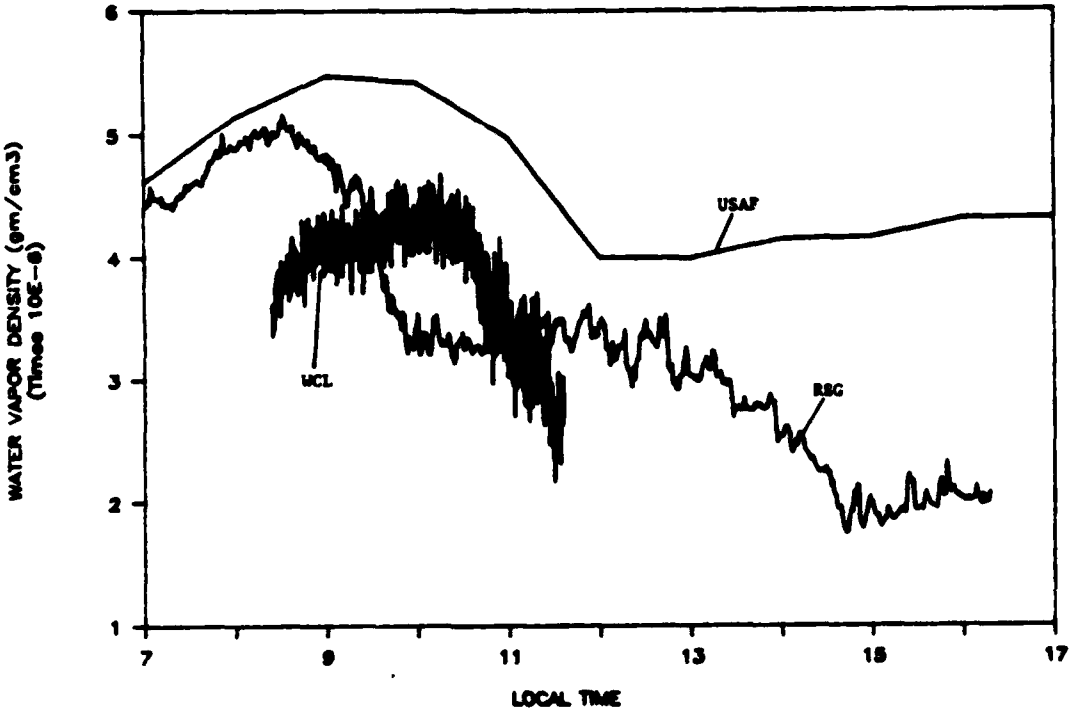

Figure 3.7 Comparison of Surface Water Vapor Density Variation with Time Computed Using Three Independent Data Sources

Using the water vapor density at the surface at the time of satellite overpass, the integrated water vapor content can be estimated by assuming one of the standard vertical profiles for water vapor. The accuracy of this method is of course dependent on a prior knowledge of the most suitable water vapor profile, which is essentially the very quantity being sought. Use of the standard profiles does not always yield an accurate estimation of water vapor content in the southwestern United States. Table 3.3 contains results of such estimates using three standard atmospheric profiles, the US62, Mid-Latitude Summer and the Mid-Latitude Winter. The results presented are from data collected during five calibration campaigns. Also included are radiosonde-derived values for integrated water vapor

content. The units used for water vapor content are g/cm,^{2} which are equivalent to precipitable centimeters (McClatchey et al. 1972).

Table 3.3 Comparison of Estimations of Integrated Water Vapor Content Computed Based on Surface Conditions

Date	Radiosonde	US62	Mid-Lat Summer	Mid-Lat Winter
5 May 87	1.05	0.80	0.69	0.80
6 May 87	1.32	0.80	0.69	0.80
13 June 87	2.63	1.57	1.36	1.58
14 June 87	2.92	1.69	1.47	1.71
17 July 87	1.31	1.16	1.00	1.17

Under most conditions these estimates based on surface conditions do not agree well with values actually measured, particularly when actual water vapor content is large. The largest source of error for the surface relative humidity measurements is the fact they are highly dependent on very localized conditions. Local irrigation or evaporation can affect them. This is not to imply that factors such as irrigation can affect the actual atmospheric integrated water vapor content. Analysis for TM4 using the 5S code indicates that an error of 1 g/cm^2 in the integrated water vapor content, the maximum error indicated in Table 3.3, results in an error in apparent radiance at the satellite on the order of two percent. The magnitude of the error does not appear to depend on the surface reflectance. Table 3.3 illustrates the necessity of being able to determine values for integrated water vapor content from direct measurements of the atmosphere.

Autotracker Measurements

A value for integrated atmospheric water vapor content can be estimated using the Autotracker's spectral bands at 0.86 μm, 0.95 μm and 1.04 μm. Since both of the Autotracker's detectors are used for these bands, two estimates for water vapor content can be calculated.

This technique exploits the fact that no gaseous absorption takes place at 0.86 μm and 1.04 μm, reference Table 1.2. Total optical depths are determined for those bands using the Langley-Bouguer technique. Computed values for Rayleigh optical depth are then subtracted to obtain the aerosol optical depth at each wavelength. The Ångström wavelength exponent (α) can then be computed using the following relation,

$$\alpha = \left[\frac{\mathrm{Log}\left[\frac{\delta_{\mathrm{Mie},0.86}}{\delta_{\mathrm{Mie},1.04}} \right]}{\mathrm{Log}\left[\frac{0.86}{1.04} \right]} \right] . \tag{3.4}$$

Accordingly, aerosol optical depth at 0.95 μm can then be estimated by,

$$\delta_{\mathrm{Mie},0.95} = \delta_{\mathrm{Mie},1.04} \times \left[\frac{0.95}{1.04} \right]^{\alpha} . \tag{3.5}$$

In the 0.95 μm water vapor band, Beer's Law can be rewritten as,

$$V = V' e^{-m(\delta_{\mathrm{Ray}} + \delta_{\mathrm{Mie}})} t_{H_2O} . \tag{3.6}$$

Rewriting equation (3.6) yields,

$$V' = \frac{V}{e^{-m(\delta_{\mathrm{Ray}} + \delta_{\mathrm{Mie}})} t_{H_2O}} . \tag{3.7}$$

Assuming the actual water vapor content is stable over the course of the measurements represented in the Langley-Bouguer plot, the absorption due to water vapor can be removed. Files of computed transmittance values for various values of the m-u product, where m is the airmass and u is the water vapor content in g/cm^2, can be generated using either 5S or LOWTRAN for Band 8 of the Autotracker. The technique used is to iterate the value of transmittance in order to calculate a constant value for V', defined by equation (3.7), as evidenced by a slope

of zero in a plot of V′ versus airmass. Finding the correct transmittance will lead directly to the correct water vapor content using the transmittance file described above. If the initially assumed value of water vapor content is less than the actual value, the slope of the line will be negative and the assumed value is adjusted accordingly. When the slope of the line representing V′ values computed for each point in original Langley-Bouguer plot becomes zero, the water vapor content is considered to have been successfully retrieved. Figure 3.8 is an illustration of a typical zero slope line which results when this technique is employed. The intercepts of these lines should be stable from day to day because the effects of water vapor absorption have been accounted for. The FORTRAN program which executes this algorithm is found in Appendix A, entitled NCAL8.

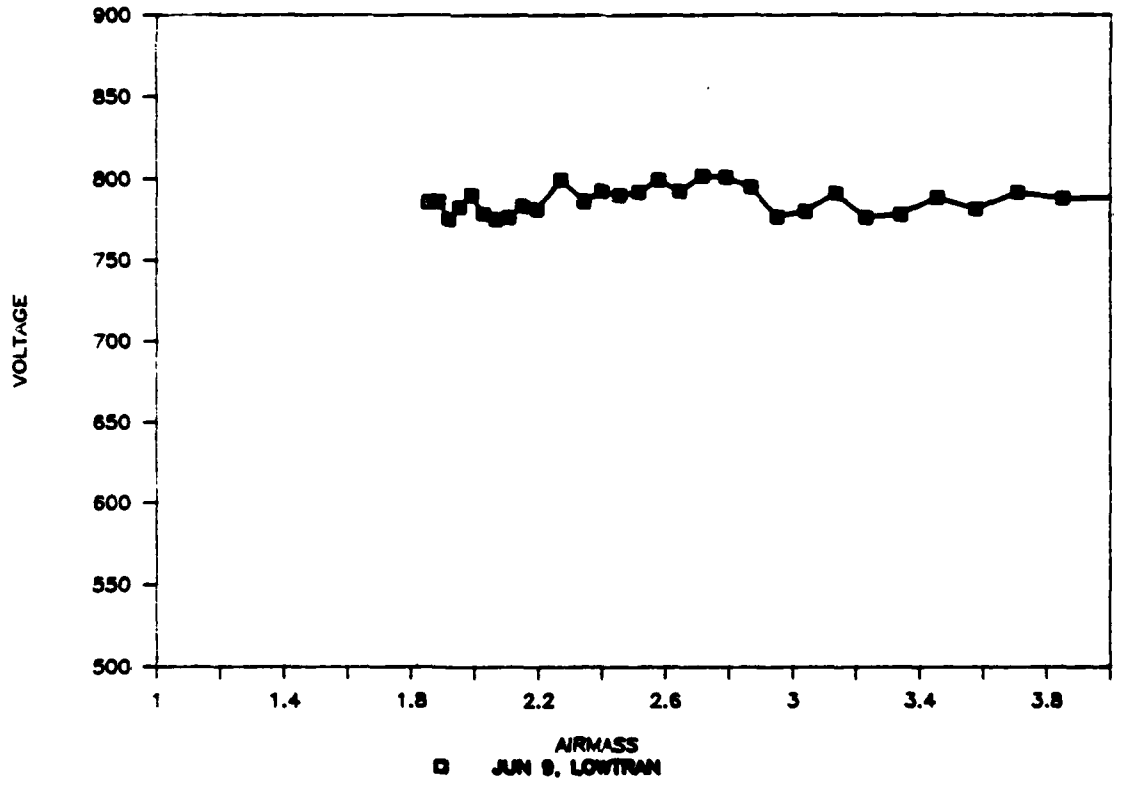

Figure 3.8 Typical Zero Slope Result from NCAL8

There were some differences in the results obtained using the 5S-generated transmittance file versus the LOWTRAN-generated transmittance file. This was due to the differing estimate of water vapor transmittance between the two codes. Figure 3.9 is a graph of the transmittance values generated by each code for m-u products from 0.1 to 20.0 for the Autotracker band at 0.95 μm. The 5S program can be seen to compute a higher transmittance for large m-u products. This probably represents overestimation of the transmittance of atmospheric water vapor.

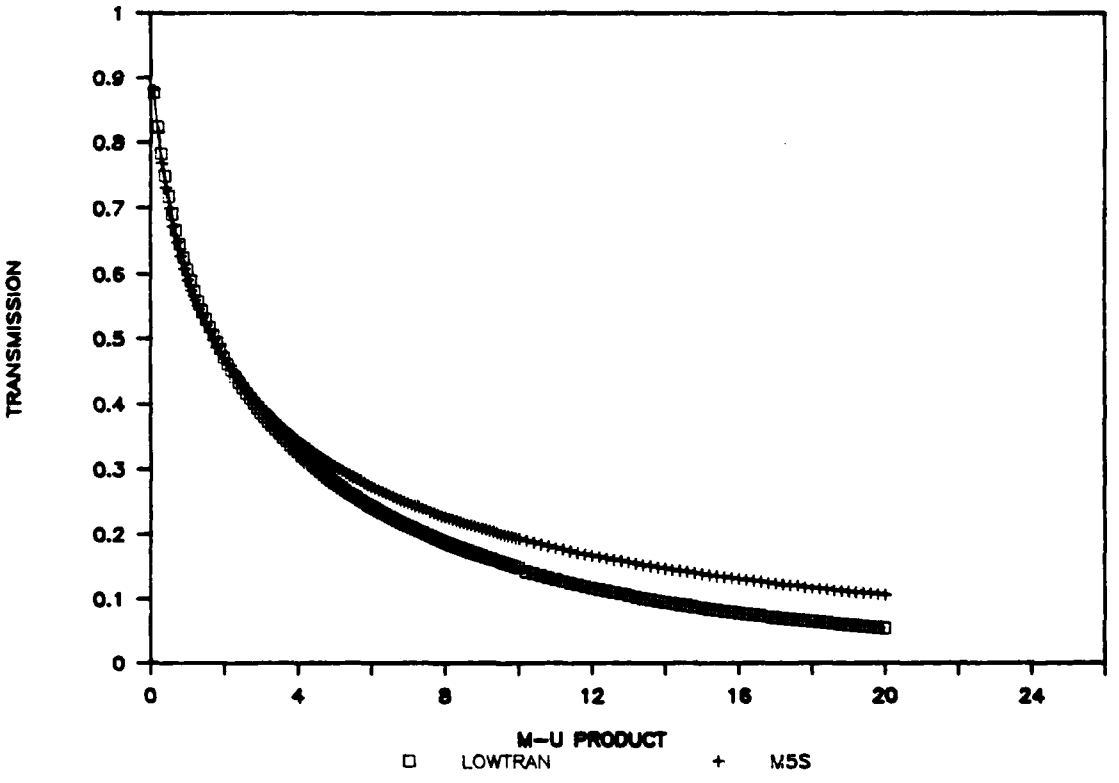

Figure 3.9 Comparison of Water Vapor Transmittance Values Generated Using 5S and LOWTRAN for Autotracker Band 8

Figure 3.10 is a graph of quasi-monochromatic water vapor transmittance calculated using the two codes from 0.93 μm to 0.97 μm, based on the Mid-Latitude Summer atmospheric model. 5S results are depicted by squares and LOWTRAN results by crosses. Also plotted as a solid line is the spectral response of the Autotracker's Band 8. The most significant differences in computed transmittance appear to occur in the wings of the band.

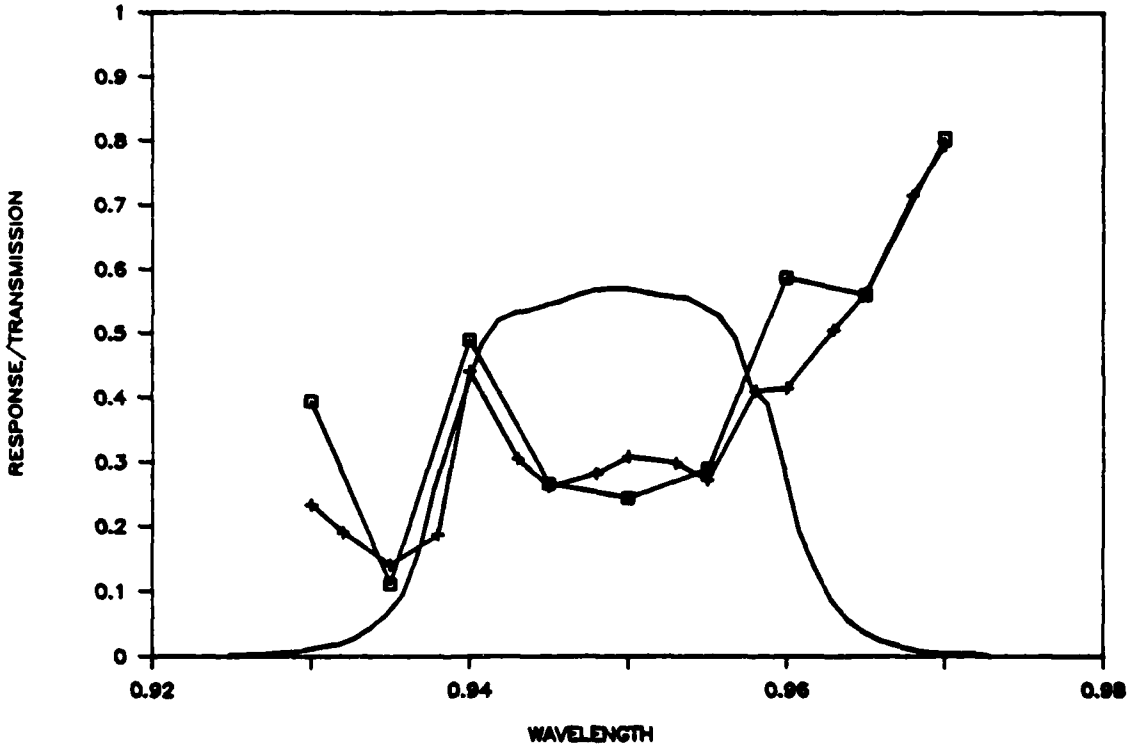

Figure 3.10 5S (□) and LOWTRAN (+) Quasi-Monochromatic Water Vapor Transmittance Values for Autotracker Band 8

Presented in Table 3.4 are the water vapor contents computed using this technique for five satellite calibration dates. Included in the table are the water vapor contents computed using both the 5S and LOWTRAN transmittance files, and using optical depths computed using data from both Autotracker detectors. For comparison the values for integrated water vapor content computed from radiosonde

data are also included. The water vapor content is expressed in g/cm². Using surface water vapor density temporal stability as the criterion, the atmospheric water vapor content was most stable on 6 May 1987 and 13 June 1987. It should be noted that the surface water vapor density was unstable on 5 MAY 1987, possibly indicating an unstable integrated water vapor content and resulting in the erroneous results from NCAL8 for that date.

Table 3.4 Results of Water Vapor Content Determination Using Band 8 of the Autotracker

		Silicon		Lead Sulfide	
Date	Radiosonde	LOWTRAN	5S	LOWTRAN	5S
27 March 87	0.43	0.47	0.50	0.51	0.56
5 May 87	1.05	0.64	0.65	0.63	0.64
6 May 87	1.32	1.25	1.78	1.20	1.70
13 June 87	2.63	2.71	5.07	2.44	4.30
14 June 87	2.92	2.44	4.25	2.14	3.54

Under most conditions use of the LOWTRAN transmittance file appears to allow calculation of an integrated water vapor content which agrees within 10 percent of that computed from the radiosonde data.

The high values of water vapor content computed using the 5S transmittance file are to be expected based on results depicted in Figure 3.9. Also, intercept values computed when the 5S transmittance file was used are not consistent over time. Figure 3.11 is a plot of the normalized zero slope intercept values calculated using the two codes for the five dates listed in Table 3.4. When compared to Figure 2.9, the LOWTRAN intercepts are seen to more closely follow the trend of the instrument overall. The 5S intercepts are, on the other hand, very erratic.

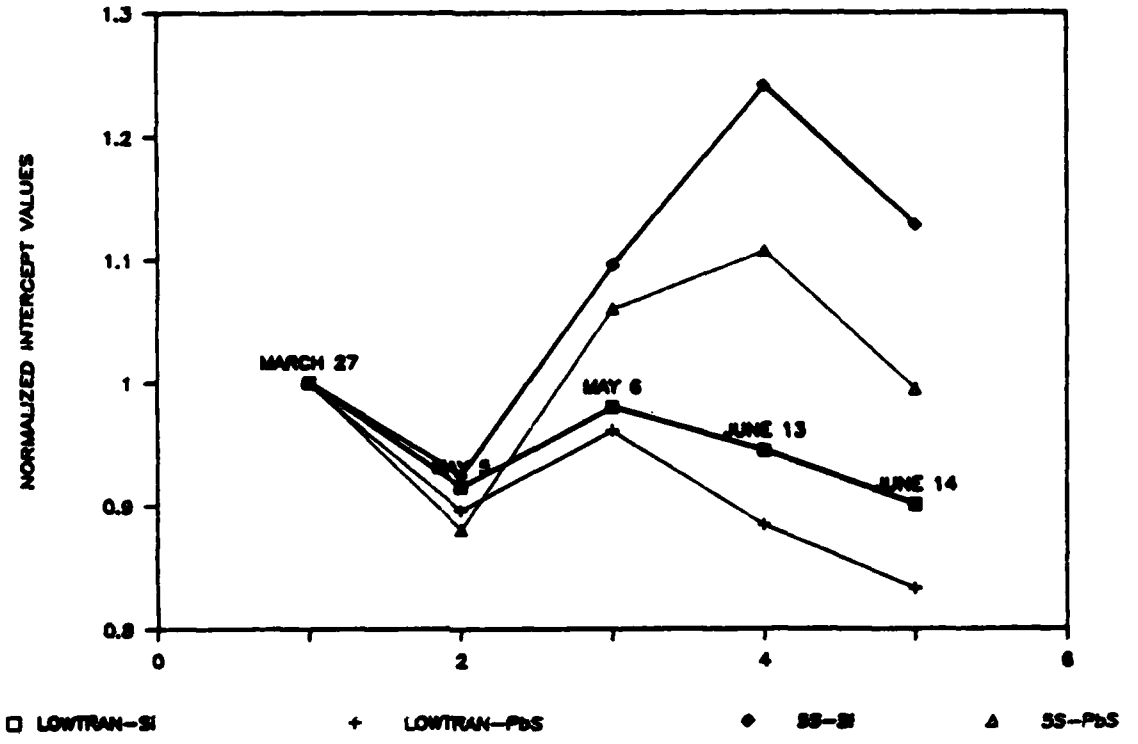

Figure 3.11 Autotracker Band 8 5S and LOWTRAN Normalized Zero Slope Intercept Values

The results obtained using the 5S transmittance file do not appear to be accurate using this technique. The reason for this may be that 5S's 5 nm resolution is too wide to accurately calculate water vapor transmittance in this relatively narrow band. This result does not necessarily have any bearing on the accuracy of 5S results in the wide atmospheric windows. This topic will be examined in Chapter 4.

Summary

From this analysis it can be concluded that the integrated water vapor content is the quantity of interest for the purpose of making atmospheric corrections and not the specific vertical distribution. Values of integrated water vapor content calculated using Band 8 of the Autotracker in conjunction with the LOWTRAN transmittance file appear accurate to 10 percent. No other available method appears to be as accurate, with the exception of methods using data collected by radiosondes launched close to the satellite calibration site and overpass time.

Under most conditions the current method of atmospheric ozone content determination is accurate to within 10 percent. Somewhat more reliable results might be possible using measurements made in the ultraviolet. Estimates of ozone content based on historical data do not appear accurate enough for satellite calibration work.

CHAPTER 4

NEAR INFRARED MEASUREMENTS

The Autotracker's spectral range in the near-IR was extended beyond its original limit of 1.04 μm through addition of a lead sulfide detector and appropriate spectral filters. The purpose of this chapter is to discuss work begun on calibrating the instrument in these near-IR bands. Such a calibration will be particularly useful since the Autotracker's spectral filters in Bands 10 and 11 were selected to closely match the spectral responses of TM5 and TM7 respectively.

First, an important aspect of the Autotracker's current mode of operation pertaining to infrared measurements must be examined. The lead sulfide detector operates at a temperature of 48°C. Specific information is not currently available on the responsivity of a lead sulfide detector operated at such a temperature. Another consideration is that every lead sulfide detector must be considered individually because of the variation possible from detector to detector. Lead sulfide responsivity curves are typically presented based on measurements made at 25°C. On such curves, the peak responsivity normally occurs at a wavelength of 2.5 μm with a rapid drop to zero at longer wavelengths. Based on information from IR Industries, the manufacturer of the Autotracker's lead sulfide detector, the wavelength of peak responsivity will shift to between 2.0 μm and 2.2 μm when the detector operates at 48°C.

The first subject investigated in the calibration of the instrument was the effects of using wide bandwidth spectral filters in the near IR.

Optical Depth Calculations

The Autotracker's near-IR bands, Bands 10, 11 and 12, are affected by gaseous absorption, see Table 1.2. These effects are particularly evident in Bands 10 and 11, due to their large bandwidth. For the purpose of preparing Langley-Bouguer plots in bands where gaseous absorption is present, Beer's Law may be expressed as,

$$E = E_0 \, e^{-m(\delta Ray + \delta Mie)} \, t_g \tag{4.1}$$

where t_g is the transmittance of the gaseous absorbers present. If gaseous absorbers are actually present but not accounted for, application of the Langley-Bouguer technique will result in obvious errors. Water vapor and carbon dioxide are the two primary constituents under examination here, so equation (4.1) can be rewritten,

$$E = E_0 \, e^{-m(\delta Ray + \delta Mie)} \, t_{H_2O} \, t_{CO_2} \quad . \tag{4.2}$$

Rewriting equation (4.2) results in,

$$E' = \frac{E}{t_{H_2O} \, t_{CO_2}} = E_0 \, e^{-m(\delta Ray + \delta Mie)} \quad . \tag{4.3}$$

Here E is the irradiance originally observed and E' is the value corrected for the effect of gaseous absorption. The Langley-Bouguer technique can now be applied plotting E' versus airmass.

The water vapor transmittance can be computed for each point on the Langley-Bouguer plot knowing the airmass and the integrated water vapor content. The water vapor content being determined using the techniques discussed in Chapter 3. Since the amount of carbon dioxide present depends only on the atmospheric pressure, the carbon dioxide transmittance is easily computed for each point in the original Langley-Bouguer plot. Using the 5S code, the calculated sea

level transmittance for carbon dioxide under a given set of geometrical conditions can be weighted by the ratio of the actual barometric pressure to standard barometric pressure at sea level. A computer program which makes these gaseous absorption corrections for Langley-Bouguer plot data is found in Appendix A, entitled BD11CAL.BAS. The program requires a table of water vapor transmittance values based on the m-u product, discussed earlier, and a table of carbon dioxide transmittance values based on the product of airmass and carbon dioxide content.

It is possible to define an optical depth due to water vapor and carbon dioxide absorption at a given wavelength, using the relation,

$$\delta_g = -\left[\frac{\ln t_g}{m}\right] \tag{4.4}$$

for an airmass value of one. Application of such optical depths generally results in lower estimates for aerosol optical depth at the affected wavelength than those obtained using the correction method outlined above, if we assume an exponential law for the absorption. This represents an overestimation of the effects of gaseous absorption, particularly in the wide spectral bands. Table 4.1 contains optical depths for three satellite calibration dates from the Autotracker's two wide near-IR spectral bands. It is important to note that for these three dates considered in chronological order, water vapor content increases significantly from one to the next. For both spectral bands, column one contains values for total optical depth obtained by correcting the Langley-Bouguer plots for gaseous absorption and column two contains total optical depth values obtained by applying a correction based on using an optical depth for water vapor and carbon dioxide. It is important to note that the comparison between the two approaches becomes increasingly poor as the actual water vapor content increases and will lead to incorrect estimates of the aerosol optical depth, primarily for conditions of high visibility.

Table 4.1 Comparison of Corrected Near-IR Total Optical Depths for Autotracker Bands 10 and 11, Based on 5S Transmittance Values

Date	Band 10		Band 11		u_{H_2O}
	Col. 1	Col. 2	Col. 1	Col. 2	
27 March 87	0.0503	0.0452	0.0263	0.0275	0.43
6 May 87	0.0440	0.0321	0.0326	0.0237	1.32
14 June 87	0.0334	0.0144	0.0184	0.0010	2.92

The transmittance files used in preparation of Table 4.1 were generated by the 5S code. The discrepancy between water vapor transmittance values calculated by 5S and LOWTRAN exists in all the Autotracker's near-IR spectral bands. Accordingly, the choice for the source of water vapor transmittance values will affect the value of optical depth attributed to aerosols in the near IR. This problem is less critical when optical depths are high. Carbon dioxide transmittance values from the two codes compare well and therefore there is little uncertainty associated with these values. Figure 4.1 is a plot of the water vapor transmittance values calculated by both codes for Autotracker Band 11 and the results of the two codes can be seen to differ significantly for this band. Which curve is more correct has not been determined. However, if LOWTRAN-generated transmittance values are used to make the correction for gaseous absorption using either method described above, the result is negative values for total optical depths on 14 June 1987. This indicates LOWTRAN overestimates the amount of absorption in this band. Since this casts some doubt on the accuracy of LOWTRAN-generated transmittance values in these spectral bands, only 5S results will be presented in the following section.

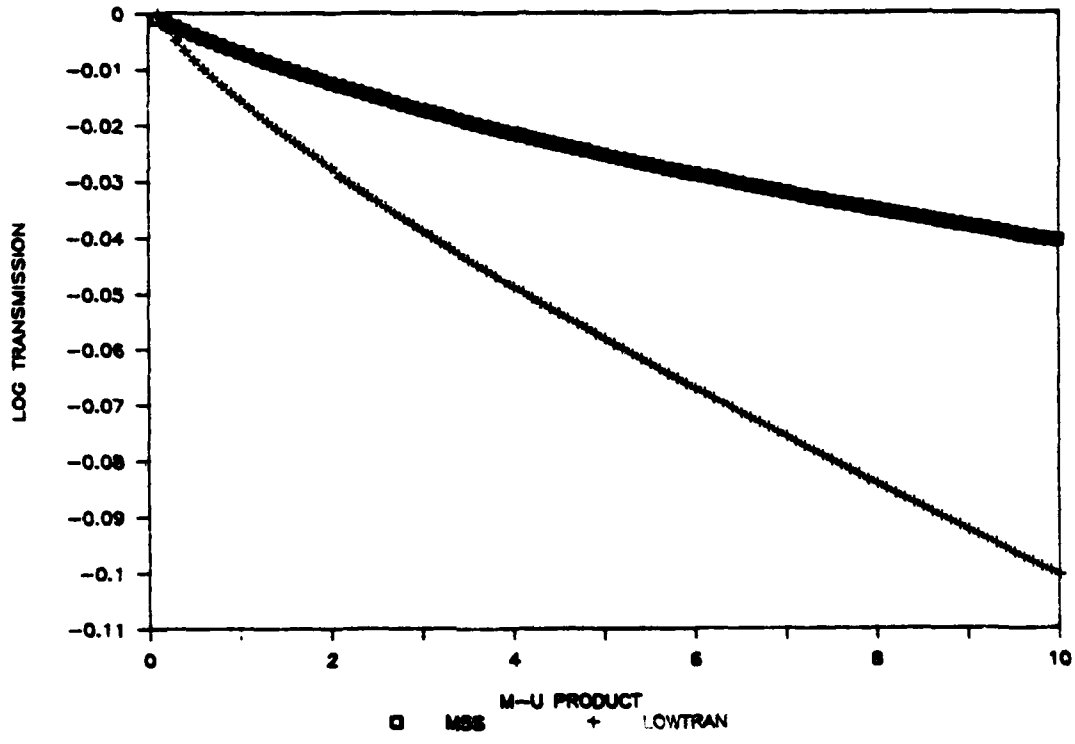

Figure 4.1 Comparison of 5S and LOWTRAN Water Vapor Transmittance Values for Autotracker Band 11

Calibration Considerations

Future calibration of the Autotracker will rely on determination of stable intercept values. Application of the procedure to correct for the effects of gaseous absorption results in a slight improvement in the stability of intercept values in the Autotracker's near-IR bands. Figure 4.2 is a plot of the intercept values corrected for the earth-sun distance for Autotracker Band 10 for five satellite calibration campaigns. The values have been normalized based on the intercept value for 27 March 1987. The base line represents the variation in intercept value for the band at 0.44 μm. It is considered to accurately reflect changes in the performance of the instrument. The correction based on 5S transmittance values slightly improves the

stability of the intercept values for Band 10. The cause of the discrepancy in the trend between the base line and Band 10 for 6 May 1987 and 9 June 1987 is unknown. It is indicative, though, of the Autotracker's erratic past performance.

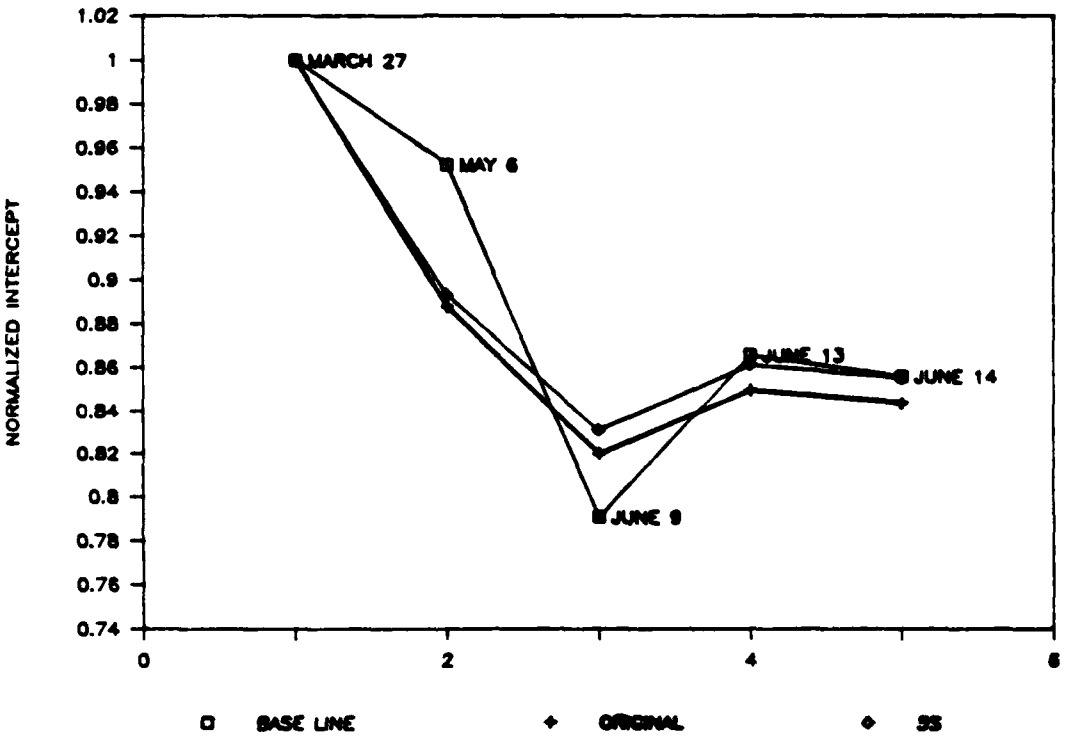

Figure 4.2 Autotracker Band 10 Normalized Intercept Values

Data collected to date suggest the possibility of using a different type of aerosol size distribution to more accurately describe the aerosols in the near-IR region. Figures 4.3 and 4.4 are Log-Log plots of δ_{Mie} versus wavelength for 27 March 1987 and 14 June 1987 respectively. In each plot the infrared bands have been corrected for the effects of gaseous absorption using a program similar to BD11CAL.BAS and 5S-generated water vapor and carbon dioxide transmittance files. The two dates were selected to illustrate both a very clear, dry day on 27 March

(calculated Junge slope of 2.55 and water vapor content of 0.43 g/cm^2) and a turbid, humid day on 14 June (calculated Junge slope of 3.95 and water vapor content of 2.92 g/cm^2) respectively. On 27 March, there is distinct evidence of two slopes on the plot. This suggests the Junge slope is not in itself sufficient to describe the aerosol size distribution on that day. However, on 14 June only one slope is evident. This is expected since days of higher optical depth have been reported to be more accurately characterized by a Junge size distribution (King et al. 1978).

The two points on each graph corresponding to the narrow and wide bands centered at 2.2 μm suggest the correction for water vapor transmittance is more accurate when the water vapor content is low. The actual difference between the two optical depths on 14 June is on the order of 0.02. Table 4.2 contains the differing results for δ_{Mie} on 27 March 1987 and 14 June 1987 for the two Autotracker bands at 2.2 μm. The first column contains results based on assuming an equivalent optical depth for gaseous absorption using 5S transmittance values. The second and third columns contain, respectively, results from using 5S and LOWTRAN-generated transmittance files to make corrections to Langley-Bouguer plot data for the two Autotracker bands at 2.2 μm using equation (4.3). The negative entries in column 3 support the concept that LOWTRAN overestimates the amount of water vapor absorption taking place in these spectral bands.

Table 4.2 Comparison of the Differing Values for δ_{Mie} Computed Based on Three Methods of Correction for Gaseous Absorption

Date	Band	δ_{Mie} ($\delta_g \rightarrow$5S)	δ_{Mie} (E'$\rightarrow$5S)	δ_{Mie} (E'$\rightarrow$LOWTRAN)
March 27	11	0.0275	0.0263	0.0192
	12	0.0249	0.0251	0.0186
June 14	11	0.0010	0.0184	-0.0182
	12	0.0321	0.0335	-0.0064

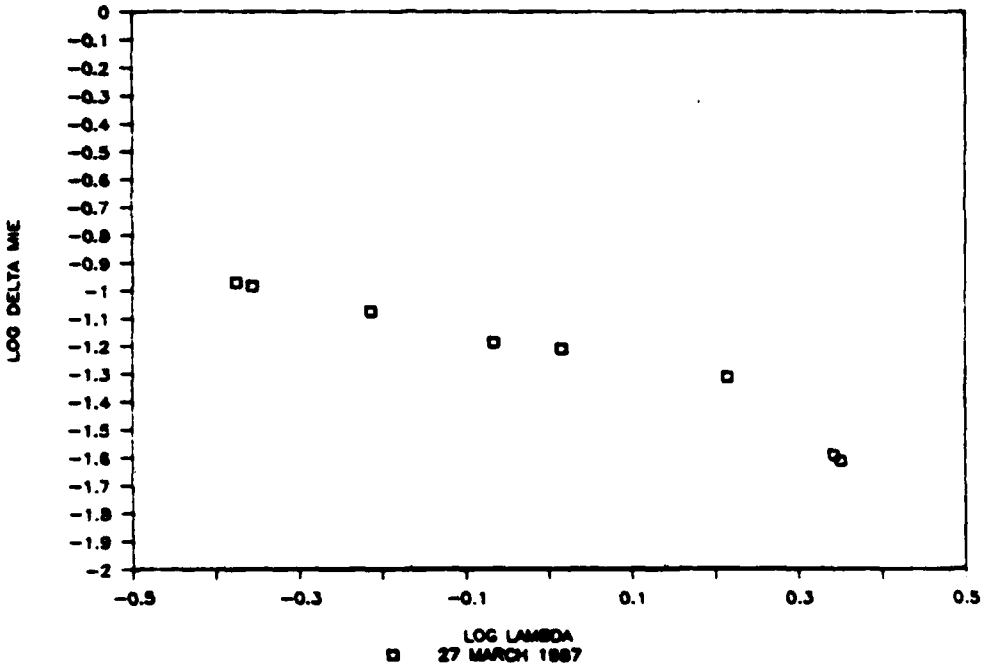

Figure 4.3 Wavelength Dependence of Aerosol Optical Depth for 27 March 1987

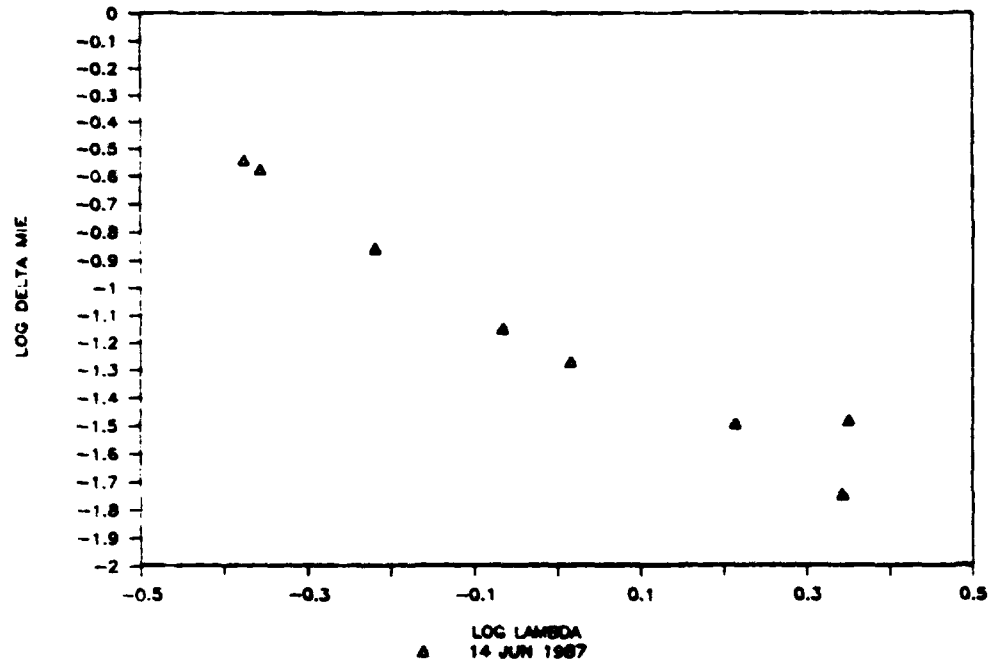

Figure 4.4 Wavelength Dependence of Aerosol Optical Depth for 14 June 1987

Summary

Before the Autotracker's near-IR spectral bands can be calibrated, their contamination by gaseous absorption must be accounted for. In order to provide valid data from which to start, the overall spectral response of the instrument at these wavelengths must be accurately defined. As discussed at the beginning of the chapter, Bands 11 and 12 of the Autotracker could be operating in a region of rapidly falling detector responsivity. This could have an impact on the results for the wide band centered at 2.21 μm. In order to obtain accurate results for this band, the wavelength dependence of the Autotracker's lead sulfide detector's responsivity must be defined through laboratory measurements. This responsivity will then have to be convolved with the spectral response of the individual bands to provide correct output voltages. In addition, the effect of the use of optical glass in the aperture window, the imaging lens and the relay lens must be considered. Glass generally begins to suffer transmission losses at wavelengths longer than 2.0 μm (Smith 1966 p.153). Therefore, in order to achieve full accuracy in Bands 11 and 12, the spectral transmittance of glasses used will have to be convolved with the spectral filter response and the detector's spectral responsivity. These corrections remain to be accomplished. The results which have been presented here were based on Autotracker data collected without these adjustments and must be considered in that light.

Once these various corrections have been made, it will be possible to perform either an absolute or inter-band calibration of the Autotracker's near-IR spectral bands in the laboratory. With such a calibration, it would then be possible to determine the gaseous transmittance for TM5 and TM7 using Autotracker Bands 10 and 11 and an airmass equal to $\frac{1}{\cos\theta_v} + \frac{1}{\cos\theta_s}$.

In addition, the introduction of an additional parameter to accurately characterize the aerosol size distribution under some conditions must be considered. Also, since the measured values of ozone content provide an accurate estimation of the actual amount of ozone present in the atmosphere, measurements in enough spectral bands are available to perform an inversion of optical depth to provide an improved estimate of the aerosol size distribution (King et. al. 1978).

CHAPTER 5

CONCLUSION: OVERALL EFFECT ON RADIANCE AT THE SATELLITE LEVEL

As a summation of this work, in this chapter the impact of the various uncertainties discussed in previous chapters on the apparent radiance observed by the satellite is examined. First, the possible errors encountered in calibration of several major satellite systems induced by inaccuracies in determination of gaseous transmittance are outlined. This is followed by an analysis of the errors associated with incorrect characterization of aerosols.

A sensitivity analysis for the various errors involved in calibration of Thematic Mapper was conducted by Kastner (1985). There are two reasons to update this study. The first is the addition of other sensors, namely SPOT and AVHRR, to the calibration process since that time. The second is the improved estimation now possible of the inaccuracies present in the various quantities involved.

For the purpose of satellite calibration calculations, it is useful to define the apparent reflectance of a target, ρ^*, by,

$$\rho^* = \frac{L^* \pi}{\mu_s E_s} \tag{5.1}$$

where L^* is the apparent radiance. Tanre' et al. (1986) have decomposed the apparent reflectance as follows,

$$\rho^* = t_g \left[\rho_A + T(\mu_s) T(\mu_v) \left[\frac{\rho}{1 - \rho\eta} \right] \right] \tag{5.2}$$

where t_g is the total gaseous transmittance and is defined by,

$$t_g = t_{O_2} \times t_{O_3} \times t_{CO_2} \times t_{H_2O} \tag{5.3}$$

ρ_A in equation (5.2) is the intrinsic atmospheric reflectance and is a function of the scattering phase function. ρ is the reflectance of the target. $T(\mu_s)$ is the global atmospheric transmittance defined by,

$$T(\mu_s) = \frac{\mu_s E_s e^{-\delta/\mu} + \Phi_d}{\mu_s E_s} \tag{5.4}$$

which represents the global flux received on a black target normalized by the incident exoatmospheric solar irradiance. The term $(1-\rho\eta)$ in equation (5.2) couples the ground and atmosphere. In this expression, η is the spherical albedo. Considering the terms in equation (5.2), t_g can presently be computed using either the 5S or LOWTRAN computer codes. ρ_A, $T(\mu_s)$, $T(\mu_v)$ and η can be computed using a radiative transfer code such as the Herman Code, discussed in Chapter 1, or by using the approximation available in 5S. In equation (5.2), scattering and gaseous absorption have been decoupled and the effects of errors in each on the apparent reflectance can be more easily analyzed.

Errors in Gaseous Transmittance

Most satellite systems attempt to avoid spectral regions of gaseous absorption as far as possible. However, particularly in the near IR, this is not always practical due to the requirement to use wide bandwidths. Wide bandwidths are required due primarily to the limited responsitivity of the detectors used.

It is necessary know the extent of the effects of gaseous absorption encountered by the spectral bands of the satellite systems of interest here as well as which absorber is primarily responsible in a given band. Table 5.1 contains the transmittances calculated for the four primary gaseous absorbers in the spectral

bands of the three major satellite systems for land remote sensing during the calibration campaign of 27 and 28 March 1987 at White Sands, New Mexico. The transmittances are those calculated by 5S for the geometrical conditions which existed at the time of overpass for each satellite. Absorber concentrations of 0.37 atm-cm for ozone and 0.43 g/cm^2 for water vapor were used for the Thematic Mapper and AVHRR calculations. For the SPOT calculations, the values used were 0.43 atm-cm for ozone and 0.5 g/cm^2 for water vapor. These were the concentrations determined to actually exist at the calibration site using the techniques discussed in Chapter 3. The first entries for each satellite are the central wavelengths and bandwidths for the individual spectral bands. These quantities were calculated using the Palmer moments method (Palmer and Tomasko 1980).

Analysis of Table 5.1 yields the following results. The Chappuis ozone absorption band mainly affects TM2, SPOT HRV 1, SPOT PAN and AVHRR Band 1. Water vapor absorption occurs primarily in TM4, TM5, TM7 and AVHRR Band 2. Carbon dioxide and oxygen absorption are residual effects. The amount of each present in a vertical column in the atmosphere depends directly on atmospheric pressure. Atmospheric pressure can be accurately measured to 0.1 millibar. In addition, the transmittance values for each computed by 5S and LOWTRAN compare well. The level of uncertainty is significantly increased for ozone and water vapor.

Calculation of accurate transmittance values for the gaseous absorbers is hampered by two problems. The first is the problem of an acceptable determination of the concentrations of absorbers present in the atmosphere and the second involves the relative accuracy of the computer codes chosen to calculate the transmittance values.

Table 5.1 Representative Gaseous Transmittance in Bands of Three Major Land Remote Sensing Satellites

	Thematic Mapper					
Band:	1	2	3	4	5	7
$\lambda(\mu m)$	0.486	0.571	0.661	0.838	1.677	2.214
$Bw(\mu m)$	0.070	0.089	0.077	0.134	0.226	0.270
t_g	0.985	0.925	0.947	0.973	0.958	0.973
t_{H_2O}	1.000	0.997	0.996	0.978	0.966	0.982
t_{O_3}	0.985	0.928	0.958	1.000	1.000	1.000
t_{CO_2}	1.000	1.000	1.000	1.000	0.992	0.991
t_{O_2}	1.000	1.000	0.992	0.995	1.000	1.000

	SPOT				AVHRR	
Band:	1	2	3	PAN	1	2
$\lambda(\mu m)$	0.549	0.653	0.840	0.624	0.633	0.847
$Bw(\mu m)$	0.107	0.081	0.118	0.228	0.130	0.286
t_g	0.917	0.928	0.977	0.919	0.898	0.891
t_{H_2O}	0.998	0.995	0.980	0.991	0.995	0.922
t_{O_3}	0.919	0.936	1.000	0.931	0.906	0.996
t_{CO_2}	1.000	1.000	1.000	1.000	1.000	1.000
t_{O_2}	1.000	0.996	0.997	0.996	0.996	0.970

Ozone

As discussed in Chapter 3, ozone content varies throughout the year, generally in a predictable manner. However, local variations in this historical pattern are possible. Such a variation could be due to a number of causes, such as an outbreak of arctic air into the interior of the continent (Grass 1987).

Table 5.2 contains the ozone transmittance values calculated by 5S for the four major satellite bands most affected by ozone. Values of ozone content for 27 and 28 March 1987 determined from the four sources discussed in Chapter 3 were used for the calculation. These values are listed in the left-hand column.

Table 5.2 Comparison of Ozone Transmittance Values for Four Major Satellite Bands Computed from Four Independent Estimates of Ozone Content, March 1987 (Concentrations in atm-cm)

	TRANSMITTANCE			
Band:	TM2	SPOT HRV 2	SPOT PAN	AVHRR 1
Seasonal: 0.293	0.942	0.954	0.955	0.925
Measured: 0.372	0.917	0.942	0.944	0.905
Reagan: 0.367	0.918	0.943	0.945	0.907
Autotracker: 0.714	0.849	0.895	0.898	0.830

The extremely high ozone content computed using Autotracker results was due to an instrument malfunction. This result has no significance other than to illustrate the effect of instrumental errors on the results of the current calculation technique. The close agreement between the ozone content directly measured and that determined from Reagan instrument data indicate that the technique currently used to calculate ozone content can be quite accurate. The difference in calculated transmittance values based on these two sources is on the order of 0.1 percent. However, if the empirically computed seasonal ozone content were used in this case, the error in transmittance would be on the order of three percent for TM2. Based on equations (5.1) and (5.2), any error in gaseous transmittance generates a similar

error in apparent reflectance or apparent radiance. Use of the seasonal value in not sufficient for accurate calibration purposes.

Water Vapor

As discussed in Chapter 3, there are a variety of sources available for the calculation or estimation of atmospheric water vapor content.

Table 5.3 contains water vapor transmittance values for the most affected bands of the three major satellite systems for which calibrations have been performed. These values apply to conditions which existed on 6 May 1987 at Edwards AFB, California at the time of overpass for each satellite. The various sources of water vapor content information are, in the order listed, radiosonde measurements, LOWTRAN-based results of the program NCAL8, 5S-based results of NCAL8 and estimates assuming the US62 vertical profile based on surface measurements made by the U.S. Air Force, the USDA WCL group and the Remote Sensing Group, the University of Arizona.

Analysis of Table 5.3 indicates that the water vapor transmittance determined from radiosonde data and that determined by NCAL8 using the LOWTRAN transmittance file compare within 0.3 percent. Use of the estimated values calculated by reference to surface conditions results in transmittance errors of about 1.5 percent for all bands but AVHRR Band 2 where the error is 3.2 percent. The surface-based estimates are too dependent on selection of the most applicable vertical profile and on variations in the local surface conditions due to irrigation etc. Radiosonde measurements are ideal, but are difficult to come by and are only very rarely made simultaneously with the satellite overpass and in close proximity to the ground reflectance measurements.

Therefore, the use of the technique used in NCAL8 promises to provide the most reliable source for water vapor content information under acceptable atmospheric conditions. Maximum accuracy of this method will require a calibration of Autotracker Band 8 in order to avoid the requirement that atmospheric water vapor content be stable during the course of the measurements. If an absolute calibration is difficult to achieve in the laboratory, an inter-band calibration remains a reasonable goal. If an absolute calibration is made, the procedure will have to be repeated periodically since the instrument's behavior is subject to variation.

Table 5.3 Comparison of Water Vapor Transmittance Values for Six Major Satellite Bands Computed from Six Independent Estimates of Water Vapor Content, May 1987. (Concentrations in g/cm^2)

		Thematic Mapper		
Source	$u(H_2O)$	TM4	TM5	TM7
Radiosonde	1.32	0.955	0.942	0.958
LOWTRAN	1.25	0.957	0.944	0.960
5S	1.78	0.946	0.933	0.948
USAF	1.17	0.959	0.946	0.962
USDA	0.7	0.971	0.958	0.975
RSG	0.8	0.968	0.955	0.972

	SPOT		AVHRR
Source	Band 3	PAN	Band 2
Radiosonde	0.960	0.984	0.878
LOWTRAN	0.961	0.984	0.881
5S	0.951	0.980	0.861
USAF	0.963	0.985	0.884
USDA	0.974	0.990	0.910
RSG	0.972	0.989	0.903

There is also the question of the choice of computer codes for the calculation of water vapor transmittance. The difference between the two codes

has been illustrated in Chapters 3 and 4. Table 5.4 contains single-pass water vapor transmittance values for three Thematic Mapper bands calculated by 5S and LOWTRAN. The two sets of conditions used were the Mid-Latitude Winter model (u_{H_2O} = 0.853 g/cm^2) with a solar zenith angle of 60^0 and the Mid-Latitude Summer model (u_{H_2O} = 2.93 g/cm^2), with a solar zenith angle of 30^0.

Table 5.4 Comparison of 5S and LOWTRAN Water Vapor Transmittance Values for TM

	TM4	TM5	TM7
		WINTER	
5S	0.958	0.947	0.962
LOWTRAN	0.947	0.899	0.913
		SUMMER	
5S	0.927	0.912	0.924
LOWTRAN	0.908	0.831	0.836

There are large discrepancies between the results of 5S and LOWTRAN, particularly in TM5 and TM7. The relative error approaches 10 percent in some cases. According to Tanre' et al. (1986), these differences are due to the different methods by which the contributions made by the wings of the spectral bands are calculated. The disagreement is accentuated by the large summer water vapor content. Clearly, the question of which program is the more accurate must be resolved to ensure accurate calibration calculations. In Chapter 4 some evidence was presented in favor of 5S concerning the correction of total optical depths for the effects of gaseous absorption in Bands 10 and 11 of the Autotracker. Also, in a systematic comparison of various gaseous transmittance calculations conducted at

the University of Lille, it was shown that the results of 5S agree well with an exact computation (Fouquart 1987).

Errors in the Aerosol Characterization

By far the most difficult task is that of correct characterization of the atmospheric aerosol content. In the present work on satellite calibration, there are three sources of error in such a characterization. These are the measured optical depth, the type of size distribution selected and the aerosol refractive index assumed.

Optical Depth Errors

During most field measurements, the Autotracker and Reagan instrument data have resulted in optical depths which differ by 0.02 at 0.52 μm. Since δ_{Ray} is considered to be known exactly, this value of 0.02 is the uncertainty in δ_{Mie}. Kastner (1985) has conducted an extensive analysis of the sensitivity of the apparent radiance to such errors. For typical conditions at White Sands consisting of a surface reflectance of 0.4 and 100 km visibility, the error in apparent radiance is on the order of 1 percent. The uncertainty in Mie optical depths in the visible expected from typical atmospheric measurements is not considered a major source of error.

Aerosol Size Distributions

Determination of the aerosol size distribution based on optical depth measurements results in an integrated value for that parameter, since the entire atmosphere is taken into account. The problem becomes one of which distribution law is the most accurate and of how many parameters are necessary to accurately describe the size distribution. Because accurate optical depth measurements made

with available instruments are still limited to wavelengths of 1.04 μm or less, the Junge size distribution based on one parameter, ν, determined from the Ångström wavelength exponent is the most applicable at this time. The results depicted in Figures 4.3 and 4.4 support this finding for wavelengths less than 1.04 μm. They also indicate the possibility of using a different aerosol size distribution model for measurements out to 2.2 μm.

The largest uncertainty in the Junge parameter ν encountered to date has been approximately 0.2. This maximum value occurred at White Sands, New Mexico in March 1987. The results of such an uncertainty on apparent radiance are listed in Table 5.5 for four TM wavelengths based on conditions which existed on 27 March 1987. These conditions included ground reflectances of approximately 0.4 for the four bands. Analysis of Table 5.5 indicates potential errors in apparent radiance associated with such an uncertainty in ν are on the order of 0.5 percent for this reflectance. If a ground reflectance of 0.05 is assumed, the apparent radiance increases for the larger value of ν with the percentage increase being slightly greater than for the case of higher ground reflectance.

Table 5.5 Comparison of Apparent Radiances Resulting from an Error in ν

$\lambda(\mu m)$	Apparent Radiance ($W/m^2/sr$) $\nu = 2.54$	$\nu = 2.74$
0.4863 (TM1)	10.33	10.28
0.5706 (TM2)	12.64	12.57
0.6607 (TM3)	10.19	10.13
0.8382 (TM4)	14.56	14.47

A reason for the small effect of uncertainty in the Junge parameter ν on apparent radiance is considered in Table 5.6. In this table $\beta_1 = 3g$, where g is an asymmetry factor defined by,

$$g = \int_{-1}^{1} \mu \, p(\mu) \, d\mu \tag{5.5}$$

where μ is the cosine of the solar zenith angle and $p(\mu)$ is the scattering phase function. In Table 5.6 ω_0 is the single scattering albedo, the result of integrating the scattering phase function over all solid angles.

Table 5.6 Compensating Results at 0.85 μm Due to Uncertainty in ν

ν	β_1	ω_0
2.54	2.0377	0.8732
2.74	1.9796	0.8846

A decreased value for ν indicates an increase in mean particle radius. As particle size increases, the asymmetry factor increases. This implies an increase in forward scattering and therefore an increase in atmospheric transmittance. However, this effect is offset by the decrease in the single scattering albedo, which is due to increased absorption by the larger particles. Particularly for high surface reflectivities, the effect of uncertainty in ν is limited. While this is true for current measurements effectively limited to wavelengths less than 1.04 μm, extension farther into the near IR requires further analysis. It must also be pointed out that this comparison was also conducted only for a fixed value of the aerosol refractive index and these results will not be valid if a variable refractive index is considered.

Further evidence of the need to improve the calculation of the aerosol size distribution through use of a different distribution is contained in Table 5.7. This table contains the date, location, δ_{Mie} for λ = 0.58 μm (TM2) and the

Ångström wavelength exponent (α) calculated for satellite calibration campaigns at White Sands, New Mexico and Maricopa, Arizona over the past several years.

Table 5.7 Comparison of Ångström Wavelength Exponent and δ_{Mie} Results from Dissimilar Locations

Location: White Sands, New Mexico					
Date	86-03-24	86-03-15	86-03-20	87-03-27	87-03-28
δ_{Mie}	0.052	0.0376	0.0418	0.0935	0.0893
α	1.12	1.51	0.17	0.72	0.37
Location: Maricopa, Arizona					
Date	85-10-27	86-03-20	86-04-21	86-04-05	86-06-24
δ_{Mie}	0.0963	0.0636	0.0464	0.0685	0.1363
α	1.43	1.74	1.53	1.36	1.57

The White Sands results are not as consistent as those from Maricopa. For instance, on March 20, 1986, on a day of very high visibility, α was found to equal 0.17. Such a value for α should indicate an abundance of large particles and a very turbid atmosphere. Also, in March 1987 at White Sands, two days with nearly equal δ_{Mie} produced a 50 percent change in α. Furthermore it appears unusual for the White Sands data to evidence an increase in δ_{Mie} with a corresponding increase in α, as would normally be expected. The single parameter of the Junge slope does not appear adequate in these cases.

The Aerosol Refractive Index

The last aspect of aerosol characterization susceptible to error is the refractive index. Kastner (1985) has shown that large errors in the real part of the refractive index have a small effect on the apparent reflectance. However, the imaginary part of the index of refraction is a critical value. This is expected since

the imaginary part of the index describes absorption by the aerosols, and therefore directly affects atmospheric transmittance calculations. Figure 5.1 illustrates this effect in a plot of apparent reflectance versus solar zenith angle. The upper three curves were prepared using unequal real parts of the refractive index, while the lower curve was generated using a different imaginary part. The ground reflectance used was 48.95 percent, typical for White Sands.

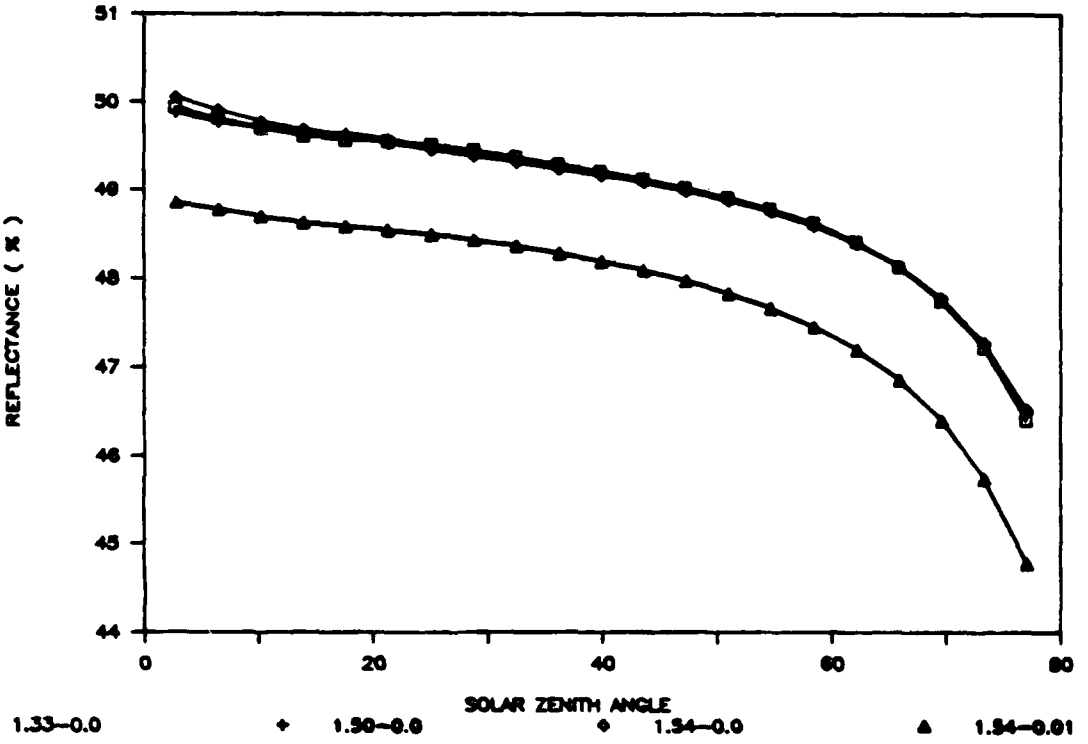

Figure 5.1 Comparison of the Effect of Varying the Aerosol Index of Refraction on Apparent Reflectance

To date, an aerosol refractive index of 1.54-0.01i has been assumed for calibration calculations. There are two types of measurements which in the future might provide more information on the refractive index and for which the necessary equipment already exists. These are a measurement of sky polarization, primarily

to determine the real part of the index and diffuse to global flux measurements, primarily to determine the imaginary part of the refractive index.

Table 5.8 contains the theoretical results of diffuse to global measurements made at a wavelength of 0.85 μm and a solar zenith angle of 70° for four values of the aerosol index of refraction. In this case the low sun elevation emphasizes the diffuse component of the flux. These calculations were made with the Successive Order radiative transfer code.

Table 5.8 Predicted Effect of the Aerosol Index of Refraction on Diffuse to Global Flux Measurements

Index	β_1	ω_0	Diffuse to Global
1.33+0.00i	2.207	1.000	0.182
1.50+0.00i	1.924	1.000	0.179
1.54+0.00i	1.862	1.000	0.178
1.54+0.01i	1.903	0.8844	0.161

The results of Table 5.8 suggest the possibility of using diffuse to global measurements at low solar elevations to determine the imaginary part of the aerosol index of refraction, regardless of the real part if the size distribution is well defined.

Figure 5.2 illustrates the possibilities for polarization measurements. It is a plot of polarization ratio in percent versus the viewing angle in degrees. These calculations were made using the Successive Order transfer code for a wavelength of 0.85 μm, in order to avoid the strong Rayleigh scattering present at shorter wavelengths, and a solar zenith angle of 70°, in order to provide access to backward scattering.

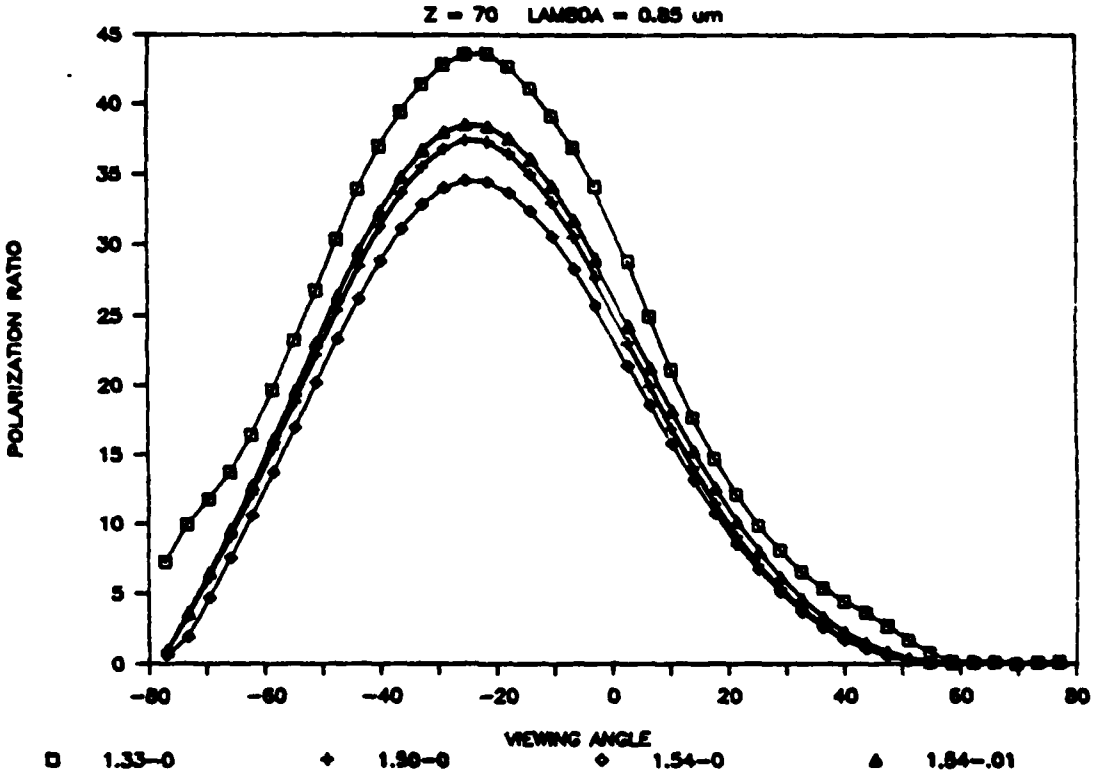

Figure 5.2 Predicted Effect of the Aerosol Index of Refraction on Observed Sky Polarization

Analysis of Figure 5.2 reveals that under these conditions the polarization ratio varies inversely with the real part of the refractive index. There is also a contribution from the imaginary part of the index as indicated by the results from the two indices with a real part of 1.54. The Autotracker was designed with the capability to make polarization measurements and may be able to make the measurements necessary for such calculations.

Summary and Recommendations

The following conclusions can be drawn concerning atmospheric measurements currently made. The error in apparent radiance associated with

errors in determination of ozone transmittance is approximately 0.1 percent. However, the error associated with the uncertainty in water vapor transmittance is on the order of one percent. For aerosol characterization, the present errors in δ_{Mie} are acceptable. However, the size distribution needs to be improved through use of near IR data. Considering their significant impact, the real and imaginary parts of the aerosol refractive index need to be determined during each calibration campaign, possibly using polarization and diffuse to global flux measurements. Polarization measurements may also help to verify the size distribution derived from optical depth measurements.

APPENDIX A

COMPUTER PROGRAMS

```
      PROGRAM TAUCM
C
      REAL MUO,L
      DIMENSION PA(26),TM(20),TR(20),TO3(20),L(20)
      DIMENSION TMC(20),TTC(20)
      DIMENSION PIO(51),BETA(51)
      CHARACTER*20 PAR
      READ(5,*)PAR,MP
C
      OPEN(UNIT=1,FILE=par)
C       INPUT OPTICAL DEPTH INFORMATION
      PI=3.14159
      READ(5,*)FOV,P,NP
      P=P+1.
      WRITE(6,*)' F.O.V.',FOV
      WRITE(6,*)' JUNGE SLOPE',P
      WRITE(6,*)' NUMBER OF WAVELENGTHS',NP
      READ(5,*)(L(I),I=1,NP)
      WRITE(6,*)'   WAVELENGTH'
      WRITE(6,31)(L(I),I=1,NP)
      READ(5,*)(TR(I),I=1,NP)
      WRITE(6,*)'   TAU RAYLEIGH '
      WRITE(6,*)(TR(I),I=1,NP)
      READ(5,*)(TM(I),I=1,NP)
      WRITE(6,*)'   TAU MIE'
      WRITE(6,*)(TM(I),I=1,NP)
      READ(5,*)(TO3(I),I=1,NP)
      WRITE(6,*)'   TAU OZONE'
      WRITE(6,*)(TO3(I),I=1,NP)
C

      XMI=100000.
      DO 1 I=1,MP
      IF(MP.EQ.21)PEO=3.45
      IF(MP.EQ.51)PEO=2.95
      PE=PEO+.05*I
      READ(1,2)BETA(I),PIO(I)
C     CHOOSE VALUES FOR AEROSOL PHASE FUNCTION
      READ(1,3)(PA(J),J=1,26)
 2    FORMAT(2(2X,E13.7))
 3    FORMAT(10E13.7)
```

```
      IF(ABS(PE-P).GE..03)GO TO 1
      IF=5*FOV+1
      DT=.2*PI/180.
      PM=0.
      PR=0.
C       COMPUTE PHASE FUNCTIONS
      DO 21 J=2,IF-1
      TETA=DT*J
      ST=SIN(TETA)
      CT=1.-ST*ST
      PM=PM+PA(J)*ST
      PR=PR+.75*(1+CT)*ST
 21   CONTINUE
      PR=PR+.75*ST*(1+CT)/2.
      PM=PM+PA(IF)*ST*.5
      PR=PR*DT
      PM=PM*DT
      WRITE(6,*)PE,PR,PM
      DO 4 J=1,NP
      TT=TR(J)+TM(J)+TO3(J)
C       COMPUTE CORRECTION FACTOR
      A=(TR(J)*PR+TM(J)*PM)/TT
      TT=TT/(1.-.5*A)
      TTC(J)=TT
C       COMPUTE CORRECTED MIE OPTICAL DEPTH
      TMC(J)=TT-TR(J)-TO3(J)
      WRITE(6,31)L(J),A,TM(J)
 4    CONTINUE
 1    CONTINUE
      DO 213 I=1,NP
      TT=TR(I)+TO3(I)+TM(I)
C       OUTPUT OPTICAL DEPTH INFORMATION
      WRITE(6,222)L(I),TT,TTC(I),TR(I),TO3(I),TM(I),TMC(I)
 222  FORMAT(7(2X,F8.4))
 213  CONTINUE
 31   FORMAT(9(2X,F8.4))
      END
```

```
5   '   R. BARTELL  21 AUG 87   WATER.BAS  DESIGNED FOR HBASIC
10  '   THIS PROGRAM CALCULATES TOTAL WATER VAPOR CONTENT IN
A
11  '   VERTICAL COLUMN BASED ON RADIOSONDE DATA
30 DIM TM(50), DEP(50),SAT(130),Z(50),DP(50),RH(50),P(50),RHO(50),SATU(130),
   TS(130),RHOP(50)
40 INPUT "ENTER SURFACE TEMPERATURE (C) ";T
50 INPUT "ENTER SURFACE FRACTIONAL RELATIVE HUMIDITY ";R
52 INPUT "ENTER SURFACE DEWPOINT TEMP IN CELSIUS ";DEW
53 INPUT "IS THE DATE OF THE DATA BETWEEN 1 APRIL AND 30 JUNE
";F
60 INPUT "ENTER INPUT FILENAME ";F1$
65 INPUT "ENTER OUTPUT FILENAME ";F2$
70 OPEN F1$ FOR INPUT AS #1
80 OPEN "SATUR.DAT" FOR INPUT AS #2
90 OPEN F2$ FOR OUTPUT AS #3
130 FOR J=1 TO 126
140 INPUT #2,TS(J),SAT(J)
150 NEXT J
160 CLS
162 KEY OFF
165 WINDOW (0,-.0000005)-(13000,.000008)
171 LINE (0,0)-(13000,0)
177 PRINT"                                        X AXIS=HEIGHT (IN m),0 - 13000"
179 PRINT"                                          Y AXIS=DENSITY (IN g/cm3), 0 -
.000008"
180 LINE (0,-.0000005)-(0,.000008)
190 RC=4615144!  'GAS CONSTANT FOR WATER
200 I=1
210 IF EOF(1) THEN GOTO 375
220 INPUT #1,Z(I),TP(I),DEP(I)
230 DP(I)=TP(I)-DEP(I)
240 TK=TP(I)+273.2
250 TD=DP(I)+273.2
260 A=(17.3*(TK-273.2))/(TK-35.9)
270 B=(17.3*(TD-273.2))/(TD-35.9)
280 ES=6.1*(EXP(A))     'CLAUSIUS-CLAPEYRON
290 E=6.1*(EXP(B))
300 RH(I)=E/ES     'SOLVE FOR RELATIVE HUMIDITY
310 FOR J=1 TO 126
320 IF TS(J)>=TP(I) THEN SATU(I)=SAT(J-1) +(((TP(I)-TS(J-1))/(TS(J)-TS(J- 1)))*(SAT(
   J)-SAT(J-1))):GOTO 340
330 NEXT J
340 P(I)=RH(I)*SATU(I)
345 P(I)=P(I)*1000  'UNIT CORRECTION
350 RHO(I)=P(I)/(RC*TK)  'SOLVE FOR DENSITY
360 PRINT #3,Z(I),RHO(I)
365 PSET(Z(I),RHO(I))
367 IF I>1 THEN LINE (Z(I-1),RHO(I-1))-(Z(I),RHO(I))
370 I=I+1: GOTO 210
375 N=I
```

```
380 FOR I=1 TO (N-1)
385 ZP=(Z(I+1)-Z(I))*100
390 RHOP(I)=ZP*(RHO(I)+((RHO(I+1)-RHO(I))/2))
400 RHOTOT=RHOTOT+RHOP(I)
401 NEXT I
403 IF Z(I+1)<12000 THEN RHOTOT=RHOTOT+((12000-Z(I+1))*(RHO(I+1)/2))
411 LINE (Z(1),RHO(1))-(Z(1),0)
412 LINE (Z(I-1),RHO(I-1))-(12000,0)
415 A$=INKEY :IF A$="" THEN 415
418 LPRINT " ":LPRINT " "
420 LPRINT "TOTAL WATER VAPOR CONTENT IN pr-cm = ";RHOTOT
490 LPRINT " ":LPRINT " ":LPRINT " "
500 LPRINT "AS A CHECK, COMPUTE LECKNER APPROXIMATION "
510 T=T+273.2
520 PS=EXP(26.23-(5416/T))
530 W=(.493*R*PS)/T
540 LPRINT "TOTAL WATER CONTENT IN pr-cm = ";W
545 LPRINT "AS ANOTHER CHECK, COMPUTE THE SMITH APPROXIMATION
"
550 IF F$="y" OR F$="Y" THEN Y=-.0229 ELSE Y=.02023
560 W=EXP((.07074*DEW)+Y)
570 LPRINT "TOTAL WATER CONTENT IN pr-cm = ";W
600 END
```

```
      PROGRAM NCAL8

      REAL     TAUTOT(2,4), TRAY(3), ALPHA, TAER, TAER1, TAER2,
LAMBDA(3),
     +     M(100), MALL(100), V(100), VALL(100), TX(100), TXALL(100),
     +     T(2,100), U, UALL, DEV, DEVALL, INTCPT, INTALL
      INTEGER  I, NGOOD, NBAD, MU
      CHARACTER*60  FILE*16(4), HEADER(5), TD*1
      LOGICAL  TIMDET(4)

   10 FORMAT (1X,A60)
   15 FORMAT (A60)
   20 FORMAT (1X,A22,F7.4,2X,F7.4)
   25 FORMAT (1X,A22,F7.2,2X,F7.2)
   30 FORMAT (1X,A14,I1,7X,A7,2X,A7)
   40 FORMAT (1X,A11,F6.4)
   50 FORMAT (A1)

      FILE(1) = 'BAND81.DAT'
      FILE(2) = 'BAND82.DAT'
      FILE(3) = 'BAND83.DAT'
      FILE(4) = 'BAND84.DAT'

      DO 220 I = 1,4
  230 WRITE (*,*) 'Do you want to use ', FILE(I), '? (Y or N) '
   READ (*,50) TD
   IF (TD .EQ. 'Y') THEN
     TIMDET(I) = .TRUE.
    ELSEIF (TD .EQ. 'N') THEN
     TIMDET(I) = .FALSE.
    ELSE
     GOTO 230
         ENDIF
  220   CONTINUE
      WRITE (*,*) ' '
      WRITE (*,*) ' '

C Read in values to fill TAUTOT array, TRAY array, and wavelengths for
LAMBDA.
C The file TAU.DAT must have the following form:
C     The first 4 rows contain tau(total) values found in the PLOT95M output
C       for each time and detector (Si am, Si pm, PbS am, PbS pm) with
C       the first value being for the lower band and second for higher band.
C     The 5th row contains tau(ray) values for each of the 3 bands in
C       ascending order of wavelength.
C     The 6th row contains the wavelengths of the 3 bands starting with
C       the lowest.

      OPEN(UNIT=1, FILE='TAU.DAT', STATUS='OLD')
      DO 100 I = 1,4
```

```
100 READ(1,*) (TAUTOT(K,I), K = 1,2)
    READ(1,*) (TRAY(K), K = 1,3)
    READ(1,*) (LAMBDA(K), K = 1,3)
    CLOSE(1)
C Read in band 8 transmittance values

    OPEN(UNIT=3, FILE='H2OB8.DAT', STATUS='OLD')
    DO 180 MU = 1,100
180   READ(3,*) (T(K,MU), K = 1,2)
    CLOSE(3)

C FOR EACH TIME/DETECTOR (1-4):
C Remove tau(r) from TAUTOT array to get tau(a) values.
C Find ALPHA; find tau(a) for band 8.
C Read the data file creating arrays for accepted data points (M,V) and
C   all data points (MALL,VALL).
C Adjust V to TX and VALL to TXALL.
C Find water vapor content (and stats) for accepted data and all data.
C Print results including tau(a) for band 8.

      OPEN(UNIT=4,FILE='MVB8.DAT')
       DO 200 I = 1,4
      IF (TIMDET(I)) THEN

C     Remove tau(r) from TAUTOT array to get tau(a) values.
   TAER1 = TAUTOT(1,I) - TRAY(1)
   TAER2 = TAUTOT(2,I) - TRAY(3)

C     Find ALPHA; find tau(a) for band 8.
   ALPHA = LOG(TAER1 / TAER2) / LOG(LAMBDA(1) / LAMBDA(3))
   TAER = TAER2 * (LAMBDA(2) / LAMBDA(3)) ** ALPHA

C     Read the data file creating arrays for accepted data points (M,V) and
C       all data points (MALL,VALL).
C     Adjust V to TX and VALL to TXALL.

    OPEN(UNIT=2, FILE=FILE(I), STATUS='OLD')
   DO 120 J = 1,5
120   READ(2,15) HEADER(J)
   READ(2,*) NGOOD
   DO 140 J = 1, NGOOD
     READ(2,*) M(J), V(J)
     TX(J) = V(J) / EXP(- M(J) * (TAER + TRAY(2)))
     MALL(J) = M(J)
     VALL(J) = V(J)
140   TXALL(J) = TX(J)
   READ(2,*) NBAD
   DO 160 J = (NGOOD + 1),(NGOOD + NBAD)
     READ(2,*) MALL(J), VALL(J)
160   TXALL(J) = VALL(J) / EXP(- MALL(J) * (TAER + TRAY(2)))
   CLOSE(2)
```

```
C     Find water vapor content (and stats) for accepted data.
        WRITE(4,*)I,NGOOD
      CALL FINDU(T, TX, M, NGOOD, U, DEV, INTCPT)
        WRITE(4,9876)(M(II),TX(II),II=1,NGOOD)
 9876   FORMAT(2(4X,F10.4))

C     Find water vapor content (and stats) for all data.
        WRITE(4,*)NGOOD+NBAD
      CALL FINDU(T, TXALL, MALL, (NGOOD + NBAD), UALL, DEVALL,
INTALL)
        WRITE(4,9876)(M(II),TX(II),II=1,NGOOD+NBAD)

C     Print results including tau(a) for band 8.
      DO 190 L = 1,3
  190   WRITE (*,10) HEADER(L)
      WRITE (*,30) 'Time/detector ', I, 'ACC PTS', 'ALL PTS'
      WRITE (*,*)  '                              ------  -------'
      WRITE (*,20) 'Water vapor content = ', U, UALL
      WRITE (*,25) 'Standard deviation  = ', DEV, DEVALL
      WRITE (*,25) 'Intercept of t/tx   = ', INTCPT, INTALL
      WRITE (*,40) 'tau(aer) = ', TAER
      WRITE (*,40) 'tau(ray) = ', TRAY(2)
      WRITE (*,*) ' '

      OPEN(UNIT=7,FILE='CALOUT',ACCESS='APPEND')
      DO 195 L = 1,3
  195   WRITE (7,10) HEADER(L)
      WRITE (7,30) 'Time/detector ', I, 'ACC PTS', 'ALL PTS'
      WRITE (7,*)  '                              ------  -------'
      WRITE (7,20) 'Water vapor content = ', U, UALL
      WRITE (7,25) 'Standard deviation  = ', DEV, DEVALL
      WRITE (7,25) 'Intercept of t/tx   = ', INTCPT, INTALL
      WRITE (7,40) 'tau(aer) = ', TAER
      WRITE (7,40) 'tau(ray) = ', TRAY(2)
      WRITE (7,*) ' '

        ENDIF
  200 CONTINUE
      END

      SUBROUTINE FINDU (T, TX, M, NPTS, U, SIGMA, INTCPT)

C  Converges on a value of U.

      REAL  T(2,100), TX(100), M(100), U, SIGMA, INTCPT, STOL, UMAX,
     +      UMIN, XMU, TINTERP, TRATIO(100)

      INTEGER  J, MU, NPTS, COL

      STOL = .01
```

```
      UMAX = 6.
      UMIN = 0.

  100 U = (UMAX + UMIN) / 2.
      DO 200 J = 1, NPTS
     COL = 1
     XMU = 10. * M(J) * U
     IF (XMU .GT. 100.) THEN
       COL = 2
       XMU = XMU / 2.
      ENDIF
     MU = INT(XMU)
     TINTERP = (FLOAT(MU+1)-XMU) * T(COL,MU) +
       +       (XMU-FLOAT(MU)) * T(COL,MU+1)
  200 TRATIO(J) = TX(J) / TINTERP

      CALL LINEAR(M, TRATIO, NPTS, SIGMA, SLOPE, INTCPT)
      IF (ABS(SLOPE) .GE. STOL) THEN
     IF (SLOPE .LT. 0.) THEN
       UMIN = U
      ELSE
       UMAX = U
      ENDIF
     GOTO 100
        ENDIF
        DO 123 I=1,NPTS
  123   TX(I)=TRATIO(I)
      RETURN
      END

      SUBROUTINE LINEAR(X, Y, N, DEV, SLOPE, INTCPT)

C  Perform a linear regression on Y as a function of X, yielding the slope
C of the line SLOPE and the intercept INTCPT.  Also yield the standard
C deviation DEV.

      REAL  X(100), Y(100), DEV, SLOPE, INTCPT, SUMX, SUMY, SUMXY,
SUMX2,
     + VAR, YF
      INTEGER N, I

      VAR = 0.
      SUMX = 0.
      SUMY = 0.
      SUMXY = 0.
      SUMX2 = 0.

      DO 50 I = 1,N
     SUMX = SUMX + X(I)
        SUMY = SUMY + Y(I)
```

```
      SUMXY = SUMXY +  X(I) * Y(I)
 50 SUMX2 = SUMX2 +  X(I) ** 2.

    SLOPE = (N * SUMXY  -  SUMX * SUMY) / (N * SUMX2 - SUMX**2.)
    INTCPT = (SUMX * SUMXY - SUMX2 * SUMY) / (SUMX**2. - N *
SUMX2)

    DO 60 I = 1,N
  YF = SLOPE * X(I) + INTCPT
 60    VAR = VAR + (YF - Y(I))**2
    DEV = SQRT(VAR/FLOAT(N))

    RETURN
    END
```

```
10 'R. BARTELL  20 AUG 1987   BD11CAL.BAS
20 'THIS PROGRAM ACCOUNTS FOR CO2 AND H2O ABSORPTION FOR THE
A-T
    BAND 11
30 'INPUT FILE IS BAND 11 SECTION OF THE TAPE95 FILE
35 OPTION BASE 1
40 DIM M(300),V(300),VM(300),CO2T(200),H2OT(200),MPF(200),MUF(200)
50 INPUT "ENTER ATMOSPHERIC PRESSURE (in Hg) ";AP
60 INPUT "ENTER ATMOSPHERIC WATER VAPOR CONTENT (g/cm2) ";U
70 INPUT "ENTER INPUT FILENAME ";FA$
80 INPUT "ENTER OUTPUT FILENAME ";FB$
90 OPEN FA$ FOR INPUT AS #1
100 OPEN FB$ FOR OUTPUT AS #2
110 OPEN "BD11H2O.DAT" FOR INPUT AS #3
120 OPEN "BD11CO2.DAT" FOR INPUT AS #4
130 I=1
140 IF EOF(1) THEN GOTO 180
150 INPUT #1,M(I),V(I)    'INPUT AIRMASS AND VOLTAGE VALUES
160 V(I)=EXP(V(I))          'CONVERT FROM LOG(V) VALUES
170 I=I+1:GOTO 140
180 N=I-1
200 AP=AP*33.865307#        'CONVERT in TO millibars
210 FOR J=1 TO 145          'READ IN CO2 TRANSMITTANCE VALUES
220 INPUT #4,MPF(J),CO2T(J)
230 NEXT J
240 FOR J=1 TO 150          'READ IN H2O TRANSMITTANCE VALUES
250 INPUT #3,MUF(J),H2OT(J)
260 NEXT J
270 FOR I=1 TO N
280 MP=M(I)*AP:MU=M(I)*U
290 FOR J=1 TO 145          'FIND CO2 TRANSMITTANCE VALUE
300 IF MPF(J)>=MP THEN
    CO2TR=CO2T(J-1)+(((MP-MPF(J-1))/(MPF(J)-MPF(J-1)))*(CO2T(J)-CO2T(J- 1))):
    GOTO 319
310 NEXT J
319 CO2TOT=CO2TOT+CO2TR
320 FOR X=1 TO 150          'FIND H2O TRANSMITTANCE VALUE
325 IF MUF(X)>=MU THEN
    H2OTR=H2OT(X-1)+(((MU-MUF(X-1))/(MUF(X)-MUF(X-1)))*(H2OT(X-)-H2OT
    (X- 1))):GOTO 349
330 NEXT X
349 H2OTOT=H2OTOT+H2OTR
350 VM(I)=V(I)/(H2OTR*CO2TR)
355 PRINT M(I),V(I),VM(I)
360 VM(I)=LOG(VM(I))
370 PRINT #2,M(I),VM(I)
380 NEXT I
400   PRINT "EXECUTION COMPLETE, NUMBER OF DATA POINTS
CONVERTED =
    ";N
460 M=1
```

```
470 MU=M*U:MP=M*AP
480 FOR J=1 TO 145
490 IF MPF(J)>=MP THEN
    CO2TR=CO2T(J-1)+(((MP-MPF(J-1))/(MPF(J)-MPF(J-1)))*(CO2T(J)-CO2T(J- 1))):
    GOTO 500
495 NEXT J
500 FOR X=1 TO 150
505 IF MUF(X)>=MU THEN
    H2OTR=H2OT(X-1)+(((MU-MUF(X-1))/(MUF(X)-MUF(X-1)))*(H2OT(X-)-H2OT
    (X- 1))):GOTO 520
510 NEXT X
520 DELTCO2=-(LOG(CO2TR)):DELTH2O=-(LOG(H2OTR))
530 PRINT" "
540 PRINT "DELTA CO2, A-T BAND 11 = ";DELTCO2
550 PRINT "DELTA H2O, A-T BAND 11 = ";DELTH2O
600 END
```

LIST OF REFERENCES

Almanac for Computers (1987). National Almanac Office, United States Naval Observatory, Washington, D.C.

Castle, K.R. (1985). The Absolute Radiometric Calibration of a Spectroradiometer. Ph.D. Dissertation, The University of Arizona.

Chandrasekhar, S. (1960). Radiative Transfer. Dover Publishers, Inc. New York, 393 pp.

Elterman, L. (1968). "UV, Visible, and IR Attenuation for Altitudes to 50 km, 1968." Report AFCRL 68-0153, Environmental Research Papers No. 285, Air Force Cambridge Research Laboratories, Hanscom Field, Mass.

Elterman, L. (1970). "Vertical-Attenuation Model With Eight Surface Meteorological Ranges 2 to 13 Kilometers." Report AFCRL 70-0200, Environmental Research Papers No. 318, Air Force Cambridge Research Laboratories, Hanscom Field, Mass.

Dobson, G.M.B. (1963). Exploring the Atmosphere. Clarendon Press, Oxford England. 185 pp.

Driscoll, W.G. ed. 1978. Handbook of Optics. McGraw-Hill Book Co. New York.

Federal Meteorlogical Handbook, No. 3. "Radiosonde Measurements." U.S. Department of Commerce. January 1, 1969.

Fouquart, M. (1987) Personal communication concerning comparisons of atmospheric transmittance codes.

Grass, R. (1987) NOAA Atmospheric Research Laboratory, Boulder Colorado. Private communication concerning atmospheric ozone measurements.

Herman, B.L. and S.R. Browning (1965). "A Numerical Solution to the Equation of Radiative Transfer." J. Atmo. Sci. 22, pp. 559-566.

Herman, B.L. (1986). Classnotes for OPTI 656A, Fall Semester, 1986.

Hipps, L. (1987). Professor, Utah State University, Dept. of Soil Science and Biometeorology. Personal communication concerning saturation vapor pressures.

Iqbal, M. (1983). An Introduction to Solar Radiation. Academic Press, Inc. New York, 390 pp.

LIST OF REFERENCES--Continued

IR Industries (1987) Private communication concerning PbS responsivity temperature dependence.

Jennings, S.G., R.G. Pinnick and H.J. Auvermann. (1978). "Effects of Particulate Complex Refractive Index and Particle Size Distribution Variations on Atmospheric Extinction and Absorption for Visible Through IR Wavelengths." Applied Optics, 24, pp. 3922-3929.

Junge, C.E. (1963). Air Chemistry and Radioactivity. Academic Press, Inc. New York, 382 pp.

Kastner C.J. (1985). In-Flight Absolute Radiometric Calibration of the LANDSAT Thematic Mapper. Ph.D. Dissertation, The University of Arizona.

King, M.D., D.M. Byrne, B.M. Herman and J.A. Reagan (1978). "Aerosol Size Distribution Obtained by Inversion of Spectral Optical Depth Measurements." J Atmo. Sci., 35, pp. 2153-2167.

Kneizys, F.X., E.P. Shettle, W.O. Gallery, J.H. Chetwynd, L.W. Abreu, J.E.A. Selby, S.A. Clough, and R.W. Fenn. (1983). "Atmospheric Transmittance Radiance: Computer Code LOWTRAN 6." Report AFGL-TR-83-0187, Environmental Research Papers, No. 846, Air Force Geophysics Laboratory, Hanscom AFB, Mass.

Lindberg, J.D. and J.B. Gillespie. (1977). "Relationship between Particle Size and Imaginary Refractive Index in Atmospheric Dust." Applied Optics, 16, pp. 2628-2630.

Liou, K. (1980). An Introduction to Atmospheric Radiation. Academic Press, Inc. New York, 392 pp.

McCartney, E.J. (1976). Optics of the Atmosphere. John Wiley & Sons, New York, 408 pp.

McClatchey, R.A., R.W. Fenn, J.E.A. Selby, F.E. Volz, and J.S. Garing (1972). "Optical Properties of the Atmosphere (Third Edition)." Report AFCRL-72-0497, Environmental Research Papers No. 411, Air Force Cambridge Research Laboratories, Bedford, Mass. Also in W.G. Driscoll, ed., Handbook of Optics., McGraw-Hill, New York, Ch. 14.

Palmer, J.M. and M. Tomasko (1980). "Broadband radiometry with spectrally selective detectors." Opt. Lett., 5, p. 208.

LIST OF REFERENCES--Continued

Reagan, J.A., I.C. Scott-Fleming, B.M. Herman and R.M. Schotland (1984). "Recovery of Spectral Optical Depth and Zero-Airmass Solar Spectral Irradiance Under Conditions of Temporally Varying Optical Depth." Proceedings of IGARSS '84 Symposium, Strasborg, France.

Reagan, J.A., L.W. Thomason, B.M. Herman and J.M. Palmer (1986). "Assessment of Atmospheric Limitations on the Determination of Solar Spectral Constant from Ground-based Spectroradiometer Measurements." IEEE Transactions on Geoscience and Remote Sensing, Vol GE-24, No. 2, pp. 258-266.

Reagan, J.A. (1987) Private communication concerning detector responsivity temperature dependence.

Santer, R. (1987) Private communications concerning corrections for diffuse flux.

Shaw, G.F., J.A. Reagan and B.M. Herman (1972). "Investigation of Atmospheric Extinction Using Direct Solar Radiation Measurements Made with a Multiple Wavelength Radiometer." Journal of Applied Meteorlogy, 12, pp. 374-380.

Smith, W.J. (1966). Modern Optical Engineering. McGraw-Hill Company, New York, 476 pp.

Smithsonian Meteorological Tables, 6th Ed, (1951). Smithsonian Institution, Washington D.C.

Slater, P.N. (1980). Remote Sensing Optics and Optical Systems. Addison-Wesley, Reading, Massachusetts, 575 pp.

Slater, P.N., S.F. Biggar, R.G. Holm, R.D. Jackson, Y. Mao, M.S. Moran, J.M. Palmer, and B. Yuan (1987). "Reflectance and Radiance-based Methods for In-Flight Absolute Calibration of Multispectral Sensors." Remote Sensing of the Environment, 22, pp. 11-37.

Tanre' D., C. Deroo, P. Duhaut, M. Herman, J.J. Morcrette, J. Perbos, and P.Y. Deschamps (1986). "Simulation of the Satellite Signal in the Solar Spectrum (5S)." Laboratoire d'Optique Atmospherique, Universite des Sciences et Techniques de Lille, France.

Thomason, L.W., B.M. Herman, R.M. Shotland and J.A. Reagan (1986). "Extraterrestrial Solar Flux Measurement Limitations due to a Beer's Law Assumption and Uncertainty in Local Time." Applied Optics, 21, pp. 1191-1195.

U.S. National Weather Service (1987). Tucson International Airport. Private communication concerning calculation of relative humidity.

LIST OF REFERENCES--Continued

van de Hulst, H.C. (1957). Light Scattering by Small Particles. John Wiley & Sons, New York, 470 pp.